Development of the Capability of Testing the Accuracy of Thermal CAD Software for Electronic Circuit Design

by

Stephen W. MacQuarrie

Thesis submitted to the Faculty of the

Virginia Polytechnic Institute and State University

in partial fulfillment of the requirements for the degree of

Master of Science

in

Mechanical Engineering

APPROVED:

____
Dr. Curtis H. Stern, Chairman

____
Dr. J. Robert Mahan

____
Dr. Douglas J. Nelson

December, 1987

Blacksburg, Virginia

Development of the Capability of Testing

the Accuracy of Thermal CAD Software

for Electronic Circuit Design

by

Stephen W. MacQuarrie

Dr. Curtis H. Stern, Chairman

Mechanical Engineering

(ABSTRACT)

The capability of measuring surface temperatures of hybrid circuits at the Virginia Tech Hybrid Microelectronics Laboratory has been established. This capability provides a quantitative method for effectively evaluating thermal design software.

Surface operating temperatures were measured and predicted for an operating hybrid circuit. The temperatures were measured using an infrared thermal imaging system, which measures surface temperatures by detecting the infrared radiation emitted and reflected. The accuracy of the measurements has been quantified for variations in surface emissivity, convective cooling condition, and operating temperature range.

The most accurate temperature measurement of a one-resistor circuit was compared to the operating temperature predicted by a lumped-parameter one-dimensional heat transfer analysis. The comparison agreed within the expected limits for this simple analysis and identified areas for possible improvement both of the model and the experimental technique.

Thermal design of a circuit is critical because excessive temperatures are a common cause of circuit failure. Circuit designers rely on computer programs to

predict circuit component temperatures because of the high cost of prototype experimentation. Accurate thermal design software that is currently available is too complicated for occasional use by circuit designers. Simple, yet accurate, thermal design software is essential for this type of design, so that circuit layouts can be quickly and easily optimized.

Acknowledgements

I would like to thank Dr. Stern for his guidance throughout this research and the preparation of this thesis. As he worked to increase my understanding of heat transfer, he encouraged me with kindness and friendship. I would like to thank Dr. Mahan and Dr. Nelson for serving on my graduate committee.

I am deeply indebted to the Barnes Engineering Division of the EDO Corporation for allowing me to use their thermal imaging system. The time and energy Mr. James Fitzsimons and Mr. Jay Shepherd have given to teach me about its operation is appreciated.

I wish to thank Mr. Douglas C. Hopkins for his work in preparing the test circuit and for consultation with him on countless electrical questions. Also thanks to Dr. F. William Stephenson and the students in the hybrid microelectronics lab for their willingness to teach me about the fabrication of hybrids.

I am grateful to Mrs. Kim Hill for photographing the hybrid circuits and the test apparatus. I wish to thank Mr. Stephen Simmons for his programming help in the creation of the UNCER software. I appreciate the guidance given by Mr. Paul Rucker and Mr. Meade Coulson of ITT, Roanoke in the proper use of the infrared imager.

I would like to thank my parents for the encouragement and support they gave me to begin and complete an engineering education.

I would like to thank my wife, Barbara, and our daughter, Meghan, for their consistent encouragement throughout this academic adventure. Yes, Meghan, Daddy is finished with his paper. I love you both.

My Lord and Savior, Jesus Christ, has provided the privilege of studying at Virginia Tech. I am grateful to Him for this provision and the sure hope He has given me of life everlasting.

Table of Contents

Introduction and Literature Review 1

1.1 Introduction 1

1.2 Literature Review 3

1.2.1 Overview 3

1.2.2 Electronics Packaging 3

1.2.2.1 Hybrid Circuits 4

1.2.2.2 Experimental Techniques 5

1.2.3 The Need for Thermal Control 10

1.2.3.1 Overview 10

1.2.3.2 Increase in Device Density 14

1.2.3.3 Increase in Circuit Board Density 14

1.2.3.4 Circuit Reliability 17

1.2.4 Thermal Analysis 18

1.2.4.1 Computer-Aided Design (CAD) 18

1.2.4.2 CAD results compared with IR results 22

1.2.4.3 Thermal Analysis of Hybrids 23

1.2.5 Summary 25

1.3 Objectives of the Study 26

Experimental Uncertainty 28

2.1 Introduction 28

2.2 Planning the Experiment 29

2.3 Quantifying Temperature Measurement Uncertainty 34

2.3.1 Stage Temperature 34

2.3.2 Junction Temperature 37

2.4 Results 46

Experimental Equipment and Procedure 48

3.1 Design of Experiment 48

3.2 Implementation of Experiment 50

3.2.1 Overview 50

3.2.2 Materials and Equipment Used 50

3.2.3 Procedure 51

3.2.3.1 Phase I 52

3.2.3.2 Phase II 52

3.2.3.3 Phase III 53

3.2.3.4 Phase IV 56

3.3 Methods for Observation and Interpretation 58

Thermal Computer-Aided-Design (CAD) 60

4.1 Choice of Thermal Analysis Program 61

4.2 CAD Implementation 63

4.2.1 SPICE: Use and Limitations 63

4.2.2 Assumptions 64

4.2.3 Derivation of Junction Temperature Equations 68

4.2.4 Uncertainty in Software Prediction of Junction Temperatures 71

4.3 Results of Software Trials 73

4.4 Recommendations 77

Results **81**

5.1 Experimental 81

5.1.1 Repeatability 82

5.1.2 The Emissivity Coating 82

5.1.3 Changes in Convection Heat Transfer 85

5.1.4 Variations in Input Voltages and Temperatures 87

5.1.5 Comparison of Experimental and Analytical Results 88

5.1.6 A Thermal Image of an Operating Hybrid Circuit 93

Conclusions and Recommendations **97**

Bibliography **101**

Operation Procedures and Equipment **107**

A.1 Tools required for set-up of Barnes Imager 107

A.2 Materials required for 30 hours of Imager operation 108

A.3 Expendable Supplies replaced at intervals >30 hours 108

SPICE Operation Instructions **109**

Supplementary Imager Operation Instructions **111**

Software not chosen **114**

Specifications **118**

E.1 Barnes RM-50 Specifications 118

UNCER FORTRAN Listing **120**

Vita **129**

List of Illustrations

Figure 1. Capabilities of electronic cooling schemes (Oktay, et al., 1986) 12

Figure 2. The trend of increasing number of devices at the chip level (Chu, 1986) 15

Figure 3. Hybrid circuits: a filter circuit, the test circuit and the filter circuit tested (clockwise from left) 32

Figure 4. Thermocouple locations for the measurement of the heater stage temperature 38

Figure 5. Radiance scan of the unpowered test circuit with powder applied ... 42

Figure 6. Emissivity calculated for the unpowered test circuit with powder applied 43

Figure 7. Electrical circuit model representing the thermal resistances (nodes numbered according to SPICE format). 66

Figure 8. Thermal resistance model of the electrical circuit. 67

Figure 9. Percentage of uncertainty in the junction temperature attributable to uncertainty in the stage temperature. 75

Figure 10. Temperature contours of a 1726 ohm resistor circuit powered to 40.5 volts and mounted on a 100 C stage 79

Figure 11. Temperature contours of a 1762 ohm resistor mounted on a 98 C stage 92

Figure 12. Radiance contours of an unpowered filter circuit mounted on a 110 C stage 94

Figure 13. Temperature contours of a powered filter circuit mounted on a 110 C stage 95

Figure 14. Barnes RM-50 thermal infrared imager specifications (Barnes Manual) 119

List of Tables

Table 1. The number of devices on a chip (After Chu, 1986, Oktay et al., 1986 and Kraus et al., 1982) 16

Table 2. Thermal conductivities (average values) 31

Table 3. Stage temperature measured simultaneously with different probes . . 35

Table 4. Stage temperature measured simultaneously with different thermocouple systems 37

Table 5. Accuracy of the Barnes Engineering RM-50 Imager with CompuTherm software (Fitzsimons, 1987). 39

Table 6. Test circuit emissivities (average values) 44

Table 7. Experimental Uncertainty 47

Table 8. Input data for UNCER to calculate the uncertainty in junction temperature as a function of stage temperature. 74

Table 9. The heat transfer into and out of the resistor. 77

Table 10. Results of emissivity coating comparisons 83

Table 11. Variations in the convection heat transfer 86

Table 12. Resistor temperature increase above stage temperature as a function of power dissipated by the resistor. 89

Table 13. A comparison of predicted and measured junction temperatures for To = 98 C 91

Nomenclature

A	area (cm^2)
h	convective heat transfer coefficient (W/cm^2-K)
h_r	radiation heat transfer coefficient (W/cm^2-K)
k	thermal conductivity (W/cm-K)
$\bar{F}$	two surface gray body net view factor
I	current (A)
L	thickness (cm)
N	radiance (mW/cm^2-sr)
Q	heat flux (W)
R	thermal resistance (K/W)
R_e	electrical resistance (Ω)
T	Temperature (K)
V	voltage (V)

Greek Letters

θ	thermal resistance (°C/W)
ε	emissivity
σ	Stefan-Boltzmann constant (W/cm^2-K^4)
ωh	uncertainty in the convective heat transfer coefficient (W/cm^2-K)
ωk	uncertainty in the thermal conductivity (W/cm-K)

ωA_j uncertainty in the juntion area (cm^2)

ωL uncertainty in the thickness (cm)

ωR_r uncertainty in the radiation thermal resistance (K/W)

ωR_d uncertainty in the conduction thermal resistance (K/W)

ωR_v uncertainty in the convection thermal resistance (K/W)

ωT_a uncertainty in the ambient temperature (K)

ωT_o uncertainty in the stage temperature (K)

ωT_w uncertainty in the wall temperature (K)

ωT_j uncertainty in the junction temperature (K)

ωV uncertainty in the voltage (V)

$\omega \varepsilon_j$ uncertainty in the junction emissivity

Subscripts

a ambient

b blackbody

d conduction

j junction

m measured

o stage or conduction low temperature

r radiation

t at a specified temperature

w wall

v convection

T total

Chapter 1

Introduction and Literature Review

1.1 Introduction

Electronic circuits produce heat while performing their electrical functions. The resulting high temperatures can lead to circuit failures and, therefore, must be controlled. This is an investigative study into the evaluation of software that predicts the operating temperature of hybrid circuits. Hybrid circuits offer improved electrical performance over conventional packaging techniques for electronics, such as printed circuit boards. This improved performance of hybrids is achieved by decreasing the signal path length which also increases the packaging density and creates heat removal problems. Electrical design engineers currently use software to predict the electrical response of a circuit. As circuit density increases, designers will require additional software to predict the thermal performance of the proposed circuit design.

The current development technique for new electronic circuits is to first design the circuit to meet electronic specifications using an electronic CAD routine, to then fabricate it and, finally, to test it. This leaves the handling of heat dissipation requirements until the final stages of the process. As circuit technology has advanced, allowing the components to be made smaller and to be located in closer proximity, the heat dissipation requirements have become substantial. This miniaturization of electronics has necessitated the development of new cooling techniques and the consideration of thermal constraints earlier in the design process. Waiting until the testing stage to find "hot spots" that limit the efficiency, reliability, or lifetime of a circuit can be very costly.

The project constitutes a feasibility test for an experimental technique to evaluate computer codes for eventual inclusion of thermal considerations in the design stage of electronic circuit development. The experiments measured the surface temperature of the hybrid circuit using an infrared thermography camera; then the temperatures were compared to predictions made by the software. The following section includes a review of the literature in this area as well as a description of the trade-offs made in choosing a software package.

1.2 Literature Review

1.2.1 Overview

As a preface to studying the thermal modeling of hybrid circuits and to developing experimental procedures to verify temperature predictions, a review of the contemporary literature was undertaken. Of particular interest were thermal studies of hybrids using infrared (IR) temperature analysis.

Prior to describing published studies of infrared analysis of hybrids it is helpful to first consider some general concepts, define relevant terms, and mention literature from the related topics of electronics packaging, hybrids, and experimental techniques in the study of electronic circuits. Some of the pertinent measurement techniques used in electronics packaging, including thermocouples, liquid crystals, and infrared thermography, are reviewed. The need for thermal control in electronic circuits will then be discussed. Since thermal control is facilitated by the use of thermal design techniques, the available Computer-Aided Design (CAD) tools are described. Their application to hybrids is considered and finally the combination of CAD and thermography is considered.

1.2.2 Electronics Packaging

Electronics affect our everyday lives. The calculator is a simple example of the use of the integrated circuit (IC) in household items. When a calculator key is pushed, a switch is closed which causes electricity to flow from the battery to the

calculator's circuitry. Frequently this circuit is built into one component, the IC chip. Kraus et al.(1982) define the IC as a "group of inseparably connected circuit elements fabricated in place on or within a substrate". The current flow in the IC causes the calculation to be performed and produces heat as a by-product.

The job of the packaging engineer is to encapsulate the circuit in order to protect it from mechanical vibration, shock and stress, while simultaneously removing excess heat. Excessive amounts of heat will cause the circuit to fail before its useful life has expired. More detail is given in Section 1.2.3.

1.2.2.1 Hybrid Circuits

Present day ICs are often housed in Dual-in-Line-Packages (DIPS). A DIP is inexpensive but requires a large surface area on the printed circuit board (PCB) to which it is to be mounted. Hybrid circuits allow the ICs to be packaged more densely than PCBs to meet space limitations, as well as to decrease lead lengths which increases circuit speed. Donahoe (1986) defines a hybrid as a ceramic printed wiring board (PWB) with attached active devices such as transistors or diodes. Parks (1987) gives a broader definition: "An integration of active and passive components on the surface of an inactive, interconnective substrate." Hybrids have a greater volume efficiency, lower system weight and shorter distance between connections than conventional PCB and DIP arrangements. The ceramic materials used as substrates in hybrids have many advantages including dimensional stability, chemical inertness, and high thermal conductivity (Donahoe, 1986). The disadvantages to hybrid technology are the high cost of manufacturing start-up and additional engineering required. These two costs are expected in the implementation of any new technology at a company. In spite of these disadvantages, many people in industry expect the

use of hybrids to grow; Jardine (1985) predicts an enormous 13% annual rate through 1990.

The basic building blocks of a hybrid circuit include the ceramic substrate, the circuitry screened onto its surface and the active and passive devices attached to it. The ceramic substrate is usually 0.64-1.0 mm (0.025-0.040 inches) thick and of the order of 25 mm x 50 mm (1″x2″) in size. Larger sizes of 102 mm x 102 mm (4″x4″) are being manufactured. Mizuno (1983) discusses the trade-offs in substrate sizes. Either thick-film or thin-film processes can be used to create the conductors on the substrate. A brief, yet informative, comparison of the two processes is given by Donahoe (1986). Thompson(1985) describes both manufacturing processes in detail and explains the criteria which should be used in hybrid design. Substantial detail on thick film processing is given by Pitzele (1986). After the substrate is fabricated, active devices are adhesively bonded or soldered to the substrate.

1.2.2.2 Experimental Techniques

The temperature of the circuit is important; techniques used to measure it will now be considered. An estimate of the surface temperature can be found using liquid crystals or thermal surface paint. A more sophisticated technique, infrared thermography, involves the measurement of infrared radiation emitted from the the circuit under study. Both methods are compared to the ubiquitous thermocouple. The discussion of experimental techniques is limited to these three because they are the most widely used in electronics packaging.

Liquid Crystals: Sharpless (1984) describes liquid crystals as the best tool for temperature measurements on a PCB. His advertisement attached to Berman (1983)

offered a $245 starter kit with a limited temperature range (20°C – 80°C) . This method provides a quick temperature map of the entire surface of a hybrid. He claims that they rival IR scanning techniques in providing thermal information. For all the fancy claims this method was a dead end because his company could not be located. The phone number in New Jersey was disconnected and a search of similar companies did not provide a low-cost method for obtaining a thermal map of a large variation in temperature (20°C – 40°C) . Crystals were located that were useful over a range of 2°C to 4°C increments. Moffat (1987) describes a similar temperature mapping technique using liquid crystals. He mixed 5 paints, with different temperature ranges, to obtain a thermal map. There are limitations in mixing heat sensitive paints, for example two paints will not give a good thermal map if each uses the same color to specify a different temperature. The number of paints to be mixed together should be small, unless a sensor is included in the experiment to calibrate the wide range of isotherms that develops. This method was investigated and the start up cost was estimated at $1000 from vendors other than Sharpless. These prices were considered too high because the thermography equipment was available at no cost in the electrical engineering department.

Liquid crystals change color quickly with changes in temperature to give an overall map of the isotherms (lines of constant temperature). To obtain the same information from thermocouples would require hundreds of junctions and much more set-up time. However, liquid crystals do not provide an electrical signal that can be monitored by a computer, rather they provide a visual image. This image must be recorded on film or video media for subsequent digital image processing or visual evaluation.

Infrared Thermography: The surface temperature of a circuit can be measured by infrared thermography. Thermography was used in this study because it is a noncontact temperature measurement technique which is currently used by industry for circuit testing. The technique utilizes the fact that all bodies at a temperature above absolute zero emit radiation. An infrared camera monitors the energy emitted from surfaces of the circuit assembly. The energy emitted is detected in terms of radiance, the power per unit area per unit solid angle at the target surface (Shepherd, 1987a). Each surface in the assembly emits the monitored wavelength of radiation at an intensity that is temperature dependent. An optical system focuses the incoming radiation on a receiver which converts the radiation into an electronic signal. Accompanying system hardware and software process this signal and display the fields of temperature on a CRT monitor. The isotherms are displayed with different colors. The thermal image can be stored in digitized form for later display or for comparison of multiple images. Madding (1983) presents a good description of thermography and includes an extensive glossary of terms.

Infrared measurement techniques have many advantages over conventional thermocouple measurements when used on electronics packaging. An important feature of thermography is that it is a noncontact method, a distinct advantage over thermocouples (Vanzetti, 1972). This allows the circuit to be operational while it is being measured. In hazardous environments the operator and instrumentation are protected from dangerous voltages and high temperatures. Measurement locations do not have to be chosen prior to testing and there are no hardware limitations on the number of points at which the temperature can be measured. Thermography is simple enough to be used routinely for the examination of prototype circuit boards during the design phase; e.g., Kallis, et al. (1984). The IR technique is also fast; it scans the field-of-view in seconds. Accurate, detailed studies of small areas in

hybrids can be made because thermography equipment has measured the temperature of an area as small as 0.5 mm in diameter (cf. Vanzetti, 1972).

Along with these advantages there are several disadvantages to the IR method. The most elusive property in IR measurements is the emissivity of the material being measured. This problem is exacerbated when studying hybrids because of the many different materials used in the hybrid assembly, each with its own emissivity. Emissivity is the proportionality between the radiation emitted from of a real body and that of an ideal blackbody. Values of surface emissivities tabulated in reference books are usually given as a range of values. Frequently handbooks give conflicting values for the same material. One solution to this problem is to apply constant emissivity coatings to circuits to correct for variations in emissivity (Engelhardt and Hewgley, 1973). These coatings, removable or permanent, allow the surface to emit radiation evenly. However, these coatings can impair the hybrid's convection cooling mechanisms; thus, the circuit is not tested under operating conditions. A similar disadvantage exists when the circuit must be tested out of its package, rather than mounted in the computer or other assembly where it will eventually operate.

It is important to note that a hybrid circuit will reflect radiation from its surroundings, in addition to emitting radiation. Conway (1987) presents photographs that show the operator's face reflected off the surface being measured. Stray electromagnetic energy that enters the field-of-view of the IR camera can give erroneous readings of the temperature of the circuit.

There have been numerous studies of electronics using thermography. Griffin (1968) presented some ideas for increasing the repeatability in thermography measurements. He studied the effect of variations in the environmental temperature and vibration on the IR measurement of surface temperature. He recommended that

operators perform complete statistical calibrations on their equipment to eliminate these hardware dependent inconsistencies in measurements. He also suggested periodic updates in statistical measurements to maintain the accuracy of the measurements. He discusses the changes in emissivity over the surface of the chip. Griffin's work is detailed and precise, if his suggestions are followed the repeatability of lab data should improve.

Peterman and Workman (1967) studied the small details of defects within the die. They maintain that thermography can provide "...indirect temperature measurement of local temperature as an important variable in design, testing and analysis of semiconductor devices". They consider three emissivity correction coatings and compare their properties. For low temperature work Parson's optical lacquer is superior; 3-M Black is best for contour maps and Krylon is best suited for obtaining detailed temperature profiles. They describe two fixed IR techniques, fixed spot and fixed beam, and then compares these to the scanning techniques used by the Barnes Engineering equipment. These different techniques are also well defined by Munis and Kaplan (1983), who provide a list of the advantages and disadvantages of each. Peterman and Workman (1967) give a good general comparison of fixed and scanning IR techniques, their work describes the measurement of temperature of the devices formed on the silicon. The infrared system has the capability to measure the overall component temperature map or the temperature of one device on the component. The intent of this study is to consider the overall temperature map of a hybrid first, then subsequent investigations can study the finer details of the devices on the component.

Thermography has been used to measure the range of temperatures of the entire circuit board assembly; here preparations of the equipment are different than those used in the measurement of component temperatures. Pearson (1986) used

thermography to detect faults on PCBs where hand-probing and traditional Automatic Test Equipment (ATE), such as in-circuit testers, cannot be used since they would pierce the encapsulating coating. In this application thermography can detect a fault on a PCB by comparing the image of the bad PCB with the image of a good PCB stored in memory. Pearson recommended that the composite thermal profile of ten good PCBs be averaged for comparison. Kallis, et al. (1984) presented another approach to measuring the temperature of an assembly. The circuit was enclosed in an insulated box and the power applied for 25 min, until it reached operating conditions. With the power still on, the box was then removed in a few seconds and the IR image recorded in the next few seconds. This arrangement allowed the thermography equipment to make temperature measurements before radiation and convection heat transfer could cool the components significantly.

1.2.3 The Need for Thermal Control

1.2.3.1 Overview

Each four-fold increase in packaging density requires a new solution for removing the heat generated by the electronics, see Figure 1. The heat transfer schemes take many forms, with natural and forced air convection cooling being the most common. High density applications such as supercomputers and military electronics require complex schemes such as cold plates, air conditioning, and immersion cooling. The Cray-2 supercomputer's thermal design pushed electronics cooling beyond the limit of air cooling to immersion cooling (Elmer-DeWitt, 1985). Kraus and Bar-Cohen (1983) and Steinberg (1980) present an overview of advanced

thermal packaging techniques. Recent papers give further details into the latest cooling techniques for large computer systems. IBM's Thermal Conduction Module (TCM) uses liquid cooling in which the cooling liquid does not come in contact with the chips (Chu, 1986). Figure 1 on page 12 (Oktay, et al., 1986) indicates the capabilities of various cooling schemes. The vertical lines in this figure result from holding the coolant temperature rise to an acceptable limit across the array of components being cooled. All of these thermal control schemes are implemented to accomplish one thing: electronics that perform according to design specifications.

The thermal performance of a circuit is most often characterized by its junction temperature. At this junction transition occurs between p- and n-type semiconductor materials (Szekely, 1987). Manufacturers of ICs often suggest a 125°C limit for this junction temperature under worst-case operating conditions. Kaye (1985) cites examples of companies using a range of values between 65°C – 105°C as an upper design limit for junction temperature. The junction temperature is a function of the temperature of the environment that surrounds it. For example, an IC chip in a calculator is surrounded by plastic and air at or near room temperature. In this case the heat is removed by conduction and convection heat transfer.

In any assembly, changes in junction temperature with respect to changes in ambient temperature are determined by the thermal resistance of the electronic package. Oktay, et al. (1986) define thermal resistance as "...the rise in temperature from a heat producing component to an internal reference point divided by the power dissipation of that component. The reference is usually a point on the surface of an element containing the component". Thermal resistance, θ_{ja} or R_{ja} , is commonly given in units of °C/W . For convenience, the thermal resistance in the path from the component junction to the environment can be divided into three levels: (1) the component-, (2) the package-, and (3) the system-level resistances. The

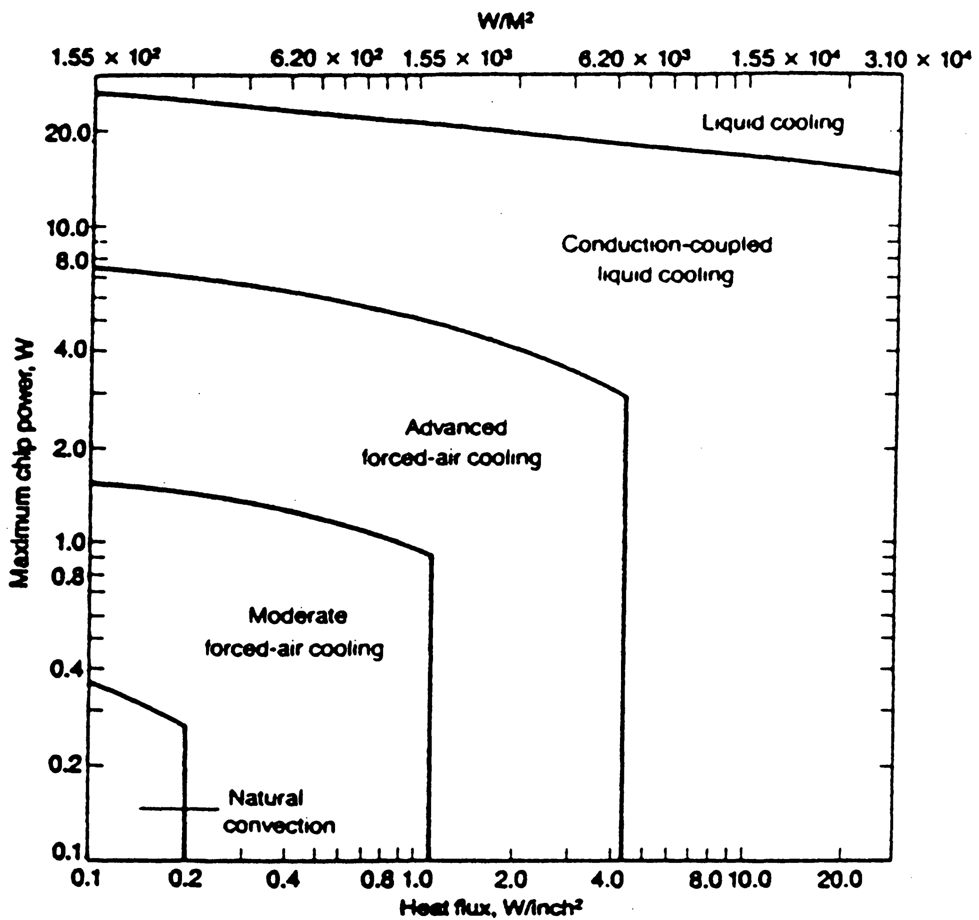

Figure 1. Capabilities of electronic cooling schemes (Oktay, et al., 1986)

component-level thermal resistance is the internal resistance between the junction and the surface of the case surrounding it. The package-level resistance exists between the case surface and some other specified location within the system. Finally, the system-level resistance refers to the path from the package or assembly level to the environment (Seely and Chu, 1972)

Kraus, et al. (1982) describe four reasons for thermal control. First, it has been shown that the reliability of a component over time decreases with an increase in junction temperature (cf. Section 1.2.3.4). The Mean-Time-Between-Failures (MTBF) is a measure used to quantify reliability. It is closely linked to the operating temperature of the device. Above a critical point the circuit the will not give the expected electrical performance. Thirdly, thermal runaway can occur after the temperature of a device passes an upper limit and a regenerative process begins. In this process the high temperatures cause the device to draw more current, which increases the temperature, which causes more current to be drawn. The cycle stops when a catastrophic device failure occurs. The fourth reason for thermal control relates to the selection of materials in the circuit assembly: solders, adhesives and the substrate material must withstand the temperatures present in the devices.

Thermal control is needed to assure that the circuit will perform reliably. There are two trends in electronic packaging which increase the power density in the assembly and, therefore, make it more difficult to cool. As electronic materials become better characterized and the circuit speed increases, more devices are built into one IC chip. This causes more heat to be generated in the component. Concurrently, recent advances in Surface-Mount Technology (SMT) and Very Large Scale Integration (VLSI) allow electronic designers to place more components on a board. These two areas will now be considered in more detail.

1.2.3.2 Increase in Device Density

The density of devices built into an IC is increasing exponentially as summarized in Figure 2. Nomenclature associated with the increasing circuit density is described in Table 1. More devices per chip means that fewer device interconnections must be made on the PCB and that the lead lengths between the devices can be made shorter. Both of these factors decrease the time required for the signal to trace out its path: faster circuitry means faster response time.

1.2.3.3 Increase in Circuit Board Density

Along with the rise in the number of devices per chip, the density of ICs on the PCB is increasing. Surface-Mounted Devices (SMDs) have been developed to reduce the amount of PCB "real estate" (surface area) required for each IC. The SMDs are soldered directly to pads on the surface of the circuit board, eliminating the need for mounting holes required by DIPs and reducing the fabrication costs. The advantage of smaller package sizes is reduced trace (lead) lengths. Shorter trace lengths have less capacitance and less inductance, which reduces the electrical current required to run the circuit. Devices with smaller power requirements have smaller turn-on times permitting faster communication between chips (Landis, 1986).

The increased density of the components on a hybrid over a PCB results from two causes; the board material and the components used. A hybrid is a circuit board made from a ceramic material such as alumina (Al_2O_3) . The ceramic material has a thermal conductivity which is two orders of magnitude greater than the glass-filled

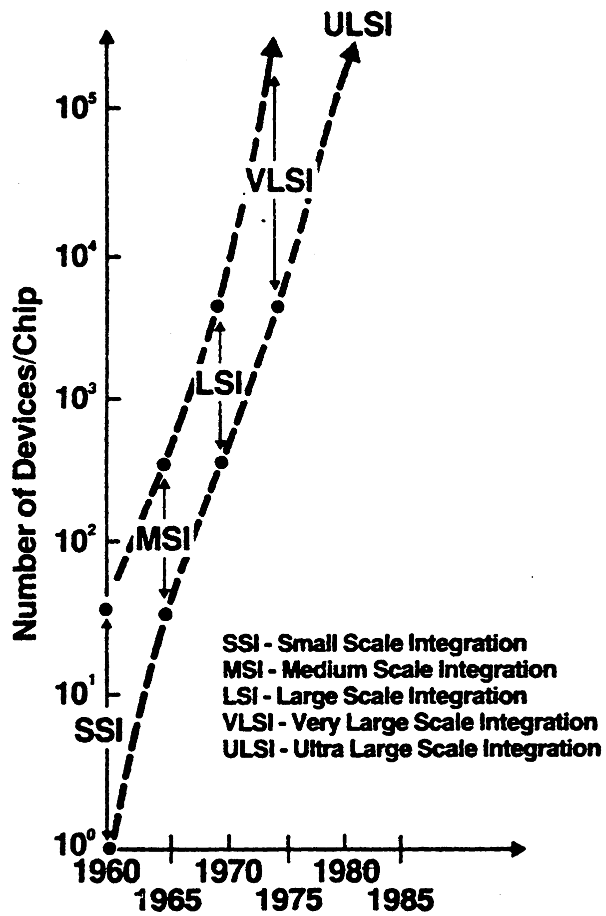

Figure 2. The trend of increasing number of devices at the chip level (Chu, 1986)

Table 1. The number of devices on a chip (After Chu, 1986, Oktay et al., 1986 and Kraus et al., 1982)

	Description	Devices Per Chip	Heat Removal (W)	Characteristic Dimension (mm)
SSI	Small Scale Integration	$< 10^2$	0.0-0.3	--
MSI	Medium Scale Integration	$10^2 - 10^3$	--	1
LSI	Large Scale Integration	$10^3 - 10^4$	1.0-3.0	--
VLSI	Very Large Scale Integration	10^4-10^5	>10	3
ULSI	Ultra Large Scale Integration	$> 10^5$	--	--

phenolic used in PCBs. The ceramic materials spread the heat quickly and this allows the circuit to be built on a smaller surface area.

The second reason hybrids are generally smaller than PCBs is the different types of component packaging schemes used. Some components are fired onto the surface of the hybrid, others are mounted with adhesives and wire bonded into the circuit, and finally SMDs are used rather than DIPs. Hybrids are used to reduce board size which increases the circuit's power density. Electronics currently supplied to the Air Force use hybrids to reduce the volume and weight of the overall electronic system (Markstein, 1984).

1.2.3.4 Circuit Reliability

Thermal studies of electronic packages must consider how the circuit will perform over time; i.e., their reliability. The circuit designer statistically computes the expected lifetime for each circuit, the Mean-Time-Between-Failures (MTBF). Kaye (1985) explains that an increase in the number of devices in the circuit reduces its MTBF. Andrews, et al. (1981) quote data which show that a 10°C increase in junction temperature reduces the device life to approximately one half. Oktay, et al. (1986) consider a 20°C change in temperature necessary for this reduction in lifetime. Regardless of the temperature rise required, circuit designers agree that the reliability is a function of temperature.

Kaye (1985) stresses the necessity of planning ahead in electronic circuit design. He advocates including the thermal aspects early in the product design cycle. Doshay (1984) also suggests such a combined thermal and electrical design approach. Software that accurately predicts device junction temperatures and circuit temperature distributions can potentially streamline the design of electronics.

1.2.4 Thermal Analysis

1.2.4.1 Computer-Aided Design (CAD)

Computer-Aided Design (CAD) is used to mathematically model the removal of heat from the circuits, because it is often cheaper and faster than the "build and test" method of design. Today, electronic components must be designed and brought to market quickly. Extensive studies of the parameters that affect the temperature of a circuit can be performed efficiently with a model that predicts the junction temperatures of devices in the circuit. Junction temperatures must be kept below a critical limit if the circuit is to function properly. Heat transfer calculations for a hybrid assembly can rarely be done analytically (Vanzetti, 1972). Therefore, it is often necessary to resort to numerical computation, using either the finite element method (FEM) or the finite difference method.

The Finite Element Method The finite element method is one of several numerical techniques used to model heat transfer in electronic circuits. Both transient and steady state analyses can be done with FEM, which was developed in the 1950s to analyze aircraft structures too complex for classical analyses. Advances in computers during the 1960s allowed this method to be applied in other areas. FEM has grown to a place of tremendous popularity in recent years as a result of the decrease in computing cost. Computers have become faster and cheaper, which makes running large FEM programs cost-effective, even for small design firms. Today, firms can employ commercial codes for their FEM analysis of heat transfer. Commonly used codes include: Ansys, Nastran, Abaqus, Adina, MARC and TAP2

(Bar-Cohen, et al., 1983). A comparison of these packages can be found in Pound (1984) and Steele (1985).

FEM has been used in many aspects of electronics analysis. For example, FEM was used with a color graphics software package to create color plots of stress in solder joints (Johnson and Seraphim, 1986). Sonnad (1983) used FEM to model fluid flow in convective heat transfer. Engel and Lim's (1986) work typifies the application of FEM to mechanical stress analysis in circuit assemblies. However, reviews of FEM's application to the problem were mixed. Marriott (1986) thought that FEM made a simple problem complex, while reducing the engineer's control over the design process. On the other hand, Schorry (1987) then replied that FEM made a complex task manageable.

The steps of the finite element calculation are described in Reddy (1984). A summary of these steps is given here. The first step is the discretization of the area to be studied into elements. Since FEM is primarily used for structures that are too complex for classical analyses, the structure is divided into small elements to permit simple mathematical description. The original users of FEM were required to painstakingly create, by hand, the element "mesh" or framework around which the model is based. This time consuming process was error prone. The meshes are now generated by preprocessor software packages that use graphics to display the mesh. Each individual point in the mesh is called a node; a group of nodes make up an element. Simple two-dimensional (2-D) elements have 3 nodes but a complex 2-D element can have as many as 32 nodes. The elements must be small enough so that the heat transfer can be accurately modeled across them. The nodes on the boundary of each element serve to connect adjacent elements. In the second FEM step, the heat transfer being studied is described accurately at each node and an interpolation function models the variation over the area of the element. Through the

interpolation function the nodal parameters are linked to the other points within the element. Because the interpolation function is dependent on the shape of the element and the number of nodes, it is unique to each element type.

The area studied can be divided into elements of many types. 2-D elements treat all heat flow in a single plane; 3-D elements consider heat flow in three dimensions. Plate and beam elements are used with geometries that can be solved by conventional plate and beam theory. Elements with nodes at their vertices allow linear variations of temperature along boundaries. In general, a large number of simple elements with linear interpolations functions must be used to accurately estimate the variation of temperature over an area. Elements with higher order interpolations functions overcome part of this disadvantage because they have nodes along the boundaries. Isoparametric elements, with side nodes, allow elements to have curved boundaries. These allow the model to be built with fewer elements. Fewer elements result in reduced computer time, but the trade-off is that each element requires more processing time (Khol, 1986).

FEM programs perform the third and subsequent steps when they generate the nodal properties and assemble these data into a matrix. After the boundary conditions and thermal loads have been included, the results are calculated and listed in tables or postprocessed and displayed in graphical form. Examples of computer generated thermal plots are shown in Pletcher and Patankar (1983).

The Finite Difference Method: The finite difference technique is also commonly used to model heat transfer in electronics. This technique is used in fluid flow analyses and other problem solutions; only heat transfer studies will be considered here. The model of a solid to be studied is divided into a grid of nodal points. The smaller the grid the more accurate the model. Finite differences are used to approximate

differential increments in the temperature and spatial coordinates. To solve for the temperature distribution simultaneous algebraic equations are written based on the fact that the heat flux at any nodal point must be zero (Holman, 1976). Temperatures are then found via an iterative solution. Preprocessors, such as CGEN, can help in creating input files (Frank and Halpern, 1983). Many commercial finite difference codes exist. Examples are: Chrysler Improved Numerical Difference Analyzer (CINDA), TAP, TOSS and TVSS2 (Rodriquez-Corre, 1984).

This same finite difference information can be rearranged and rewritten in terms of an electrical circuit which models the heat flow. This model is the same as the finite difference method mentioned above except that thermal resistances replace the thermal conductances between nodal points. In this thermal resistance network a temperature difference between nodal points is like a voltage and the heat flux through each resistor is analogous to an electric current. A solution in this form is often upgraded to solve transient problems through the use of thermal capacitances that model heat storage (Murtuza, 1982). The temperature differences can be found quickly, if they are modeled as nodal voltages by using the Simulation Program for Integrated Circuit Electronics (SPICE). This software will be discussed in detail in Chapter 4.

The personal computer (PC) and a spread sheet software package can be used to solve PDEs like the ones modeled in the finite difference method. Beccue (1987) used a spreadsheet to create simple thermal models. His models neglected radiation and convection heat losses and did not consider conductive interaction among several components on the same substrate. The heat transfer is in one dimension, but a spread angle is incorporated. These models are less complex than most FEM and finite difference analyses. Therefore, they are cheaper and faster, but less accurate. Eid (1986) also used a spreadsheet to solve the nodal equations of a

simple conduction model. He presents the nodal equations in handy tabular form with accompanying drawings.

1.2.4.2 CAD results compared with IR results

Antonetti and Simons (1985) have listed 237 publications in electronic cooling. Most were written between 1981 and 1984. Of particular interest to this study were papers combining thermal CAD and IR imaging. Baxter (1977) used CAD to predict the temperature of the junction in special test chips in an effort to standardize the reporting of thermal characteristics of standard components. Two sets of experiments were performed to verify the CAD predictions. Infrared measurements were made along with current measurements at 32 transistor junctions in the chip. He studied three types of temperatures: Junction Peak, Junction Average, and Junction Region. The Junction Peak temperature could only be measured by IR techniques and then only if the resolution of the IR lens was much smaller than the minimum junction width. Baxter also noted a lack of agreement between the CAD temperatures and IR data. The inconsistencies were attributed to reflections of the thermal radiation from the surroundings. An emissivity coating was recommended to eliminate this problem. This seemed reasonable for the measurement of radiance from a highly reflective metalization layer.

Significant (6°C – 10°C) gradients can exist within a chip between the junction and the surface of the chip or between the junction and the temperature sensing diode. This diode is built into the chip specifically for measuring the device temperature. Arnold (1982) calculated these gradients using FEM and confirmed them with IR measurements of the chip. The details of the temperature

measurements were not provided because the paper was written to describe the thermal model.

Infrared temperature measurement of semiconductors is the most widely used technique for the nondestructive measurement of temperature. For this reason it was preferred by Oettinger (1984) over four other techniques. Temperature measurements were summarized within his guidelines for the design of test chips. He compared these temperatures and some thermal resistances to those predicted by a closed form, analytical software tool, named TXYZ, which analyzes conduction heat transfer in a simple three layer structure. The comparison showed that the software gave conservative values for thermal resistance.

1.2.4.3 Thermal Analysis of Hybrids

Hybrids have been modeled by various CAD techniques in order to estimate operating parameters such as junction temperatures, heat fluxes and transient response. Walton, et al. (1981) used FEM to model the current flow in resistors and the heat flow in the substrate. They described the derivation of the equations used for FEM in great detail. The results were to be given as lines of constant temperature on a specific hybrid but this plot was not included in the paper. Frank and Halpern (1983) modeled the temperature distributions in hybrids using CGEN and CINDA. A detailed description of the software preprocessor is provided because the authors chose this as the objective for this paper. The paper presents the analyses of only one hybrid as an example of CINDA's capabilities.

Zimmer (1983) used a software package, SPICE2, to simultaneously model the thermal and electrical characteristics of hybrids. This package contains a nonlinear dependent generator that models a current source which is used to represent the

thermal power applied to the collector-emitter junction of the transistor. He used this generator to change the base-emitter voltage for a given change in the device temperature. The results of the study compare the effect of coupling the electrical and thermal characteristics of the device. A graph shows a significant decrease in the base-emitter voltage that does not occur when the thermal coupling is omitted from the model. This model is of limited value because it neglects radiation, convection and conduction coupling between power dissipating elements; only steady-state conduction is considered.

Beccue (1987) has similar restraints on the radiation, convection and conduction of his hybrid model. He sets out to create a simple, inexpensive model and could not consider all of these modes of heat transfer. This model considers steady-state conduction and its spread angle through the substrate. The computer predictions were experimentally verified for steady state operation and the agreement was within 10-20 percent for the thermal resistance of four different package types.

Buchanan and Reeber (1973) present thermal design guidelines and equations for modeling the thermal resistances, both internal and external, of hybrids. David (1977) presents a program that approximates a solution for temperature distribution in hybrids. He used a steady-state analysis because the steady-state temperature is usually the only important parameter to be predicted. He used Fourier techniques to solve Laplace's equation; convection and radiation were ignored.

Thermal Properties of Hybrids: Hybrid materials have properties that are temperature dependent. In addition, they do not dissipate power uniformly, so the conditions under which they are measured must be clearly described (Oettinger, 1984). A table of thermal conductivities of various materials, including alumina of

various purities, is provided. The change in thermal conductivity with respect to temperature for alumina is given by Baxter (1977). The thermal conductivity of alumina decreases with temperature at a rate of 3.2 percent for every 10°C between 25°C – 125°C. Beccue (1987) also lists thermal properties of materials used in hybrids. Gold (1977) gives an extensive listing of thermal properties for materials used in hybrids. Accurate properties for the new substrate material, aluminum nitride (AlN), which has 5-10 times the thermal conductivity of existing substrates and a dielectric strength similar to aluminum were not found in the literature reviewed. An additional advantage of aluminum nitride is that its thermal expansion rate is close to that of silicon (*Semiconductor International*, 1987). AlN can be expected to play a large role in the future of hybrids packaging (*Metal Progress*, 1987).

1.2.5 Summary

This review of the literature shows that there is an ever increasing need for thermal control in electronic circuits if present reliability levels are to be maintained even as power densities increase. Thermal CAD techniques are used to study the heat transfer in electronic circuits. Investigators have used both finite element and finite difference techniques, and other techniques, to model the heat transfer in hybrid circuits. Most of these models neglect the convection and radiation losses from the hybrid. The literature provides the thermal properties of hybrid materials. Computer models of the heat transfer in semiconductor chips have been verified with infrared thermal imaging. Therefore, this method is expected to be valuable in verifying the thermal analyses of hybrids.

1.3 Objectives of the Study

This study represents the initial step of a project to develop software capable of optimizing the thermal design of hybrid electronic circuits. The capability of evaluating the accuracy of thermal Computer-Aided Design (CAD) software was developed. The evaluation is accomplished by comparing the predictions with measured surface temperatures of operating circuits. The circuit temperatures were measured using an infrared thermal imaging system. The study focused on the design of thick-film hybrid circuits since this is an area of current research here at Virginia Tech.

Electrical designers need software that will predict the operating temperature of a hybrid circuit based on the operating parameters and circuit layout. With this software the designer could create thermal models of circuits on the computer which would optimize the component placement. Heat transfer in hybrid circuits must be studied to assure that components on the hybrid do not exceed their design-limit temperature. Experiments are necessary to verify the predictions of the software.

The objective of this investigation was to set up and operate the infrared imager and investigate types of thermal analysis software. The choice of a simple software model for the thermal analysis is explained and compared with the finite element and finite difference methods. Computer software was developed to predict the temperature at the junction as well as the uncertainty of the prediction. The imager was used to measure the temperature of a one-resistor test circuit. The strong influence of the stage temperature on the resistor temperature was documented along with an evaluation of the uncertainty of the temperature

measurement. Calibration tests of the imager were conducted and improvements to the temperature measurement process are described.

The imager is a highly accurate instrument for measuring the surface temperature of hybrids. An accuracy of 1°C is expected for high emissivity materials at temperatures above 100°C . Measurements were found repeatable to within 0.4°C from day-to-day. The imager and its accompanying software are capable of calculating the emissivity of the circuit materials. An emissivity coating, which raises the emissivity of many materials to approximately 0.94, was also tested. This coating was inexpensive and easy to remove. It was found to be especially useful in the temperature measurement of low emissivity materials such as silver.

Chapter 2

Experimental Uncertainty

2.1 Introduction

The experiments used in this study of heat transfer in hybrid electronic circuits involved three types of measurement. The first and second types are the mechanical dimensions of the circuit and the magnitude of the inputs to it, such as voltages and imposed temperatures. These were carefully monitored because they directly affect the third type of measurement, the output from the circuit. During hybrid operation the heat generated from the power input determines the surface temperature of the circuit. The resistor surface was chosen as this "junction" temperature, T_j, because it is the best measure of the thermal performance of the circuit. Maximum temperatures occur in the center of the resistor in the same way that maximum temperatures occur in the p-n junction of semiconductor devices. Temperature measurements cited in the literature strive to accurately measure the junction (p-n)

temperature, T_j ; therefore, the temperatures measured by the imager in this investigation are referred to as "junction" temperatures.

Uncertainties are involved in both the prediction and measurement of circuit temperatures. This chapter discusses the experimental uncertainty which is a function of the measurement accuracy of each measuring device as well as the measurement technique. The analytical uncertainty of T_j is dependent on the accuracy of parameters used with the software model. This type of uncertainty is described in Chapter 4 where the computer model is described.

The primary objective of the experiment was to measure the surface temperature of the resistor, T_j , for specified operating conditions. Measurement of this temperature provides the circuit designer with essential information. As circuits are developed, the measured temperature profile of a prototype facilitates improvement of thermal performance in future circuit designs. Temperature measurements are also valuable in verifying computer-model predictions.

2.2 Planning the Experiment

The uncertainty of the measurement of T_j and related quantities was considered prior to experimentation in order to improve the measurement accuracy and efficiency. The experimental procedure is described in Chapter 3 and the results are detailed in Chapter 5. In this chapter, the uncertainty of the measurements is discussed. Mechanical and Electrical characteristics of the test circuit were evaluated before any experiments were performed. The thermal conductivities of typical circuit materials are listed in Table 2 on page 31. A photograph of the

single-resistor test circuit is provided in Figure 3 on page 32. The circuit was designed to be simple in order to minimize the uncertainty of the junction temperature measurements made by the IR thermal imager.

Insight into the relative importance of measurement uncertainties on the T_j measurement was gained from the computer analysis (Chapter 4) done prior to the experiments. These uncertainty analyses showed that meter sensitivities had a negligible effect on the uncertainty of T_j. Two parameters surfaced as critical to the junction temperature measurement: the thermal conduction resistance, R_d , and the stage temperature, T_o. The junction temperature uncertainty, ωT_j , depends more heavily on the uncertainty of the stage temperature, ωT_o , than on the uncertainty of any other parameter. Therefore, the measurement of T_o was carefully planned in the experiment. The variation of ωT_j as a function of ωT_o is described quantitatively in Chapter 4.

The computer model showed that the majority of the heat transfer from the single-resistor circuit is by conduction. Insulation could have been placed between the resistor circuit and the imager heater stage to increase the conductive thermal resistance, thereby increasing the junction temperature. Higher surface temperatures (> 70°C) are desirable for measurement purposes because of the increased sensitivity of the IR detector. The insulation was not used because it would prohibit the emissivity correction calculations. Decreasing the conduction heat transfer is also important because changes in R_d could be accomplished easily in the laboratory and in the software model. Therefore, a range of conduction resistances, R_d , could be tested and modeled to evaluate the model accuracy. This study was planned but not executed because the imager is unable to measure the temperature

Table 2. Thermal conductivities (average values)

Material	Thermal Conductivity (W /cm C)	Temp (C)	Source	Page
Silver, Pure 99.9%	4.19	20	Holman,1976	498
Copper	3.86	20	Holman,1976	497
Gold	3.15	20	Ellison,1984	3
Aluminum alloy 3003	2.8	--	Weast,1979	D-187
Silicon	1.08	100	Weast,1979	E-15
Alumina-Al_2O_3(96%)	0.26	--	Dettmer and Charles,1987	10
Thermal grease	0.0075	--	Thermalloy Catalog,1983	48
Phenolic, glass filled	0.0045	--	Modern Plastic Encyclopedia,1985-86	457
Teflon	0.0035	--	Modern Plastic Encyclopedia,1985-86	455
Plexiglas	0.0021	--	Lynch,1975	455
Cork	0.0004	32	Holman,1976	500
Air	0.00026	20	Kays and Crawford,1980	388

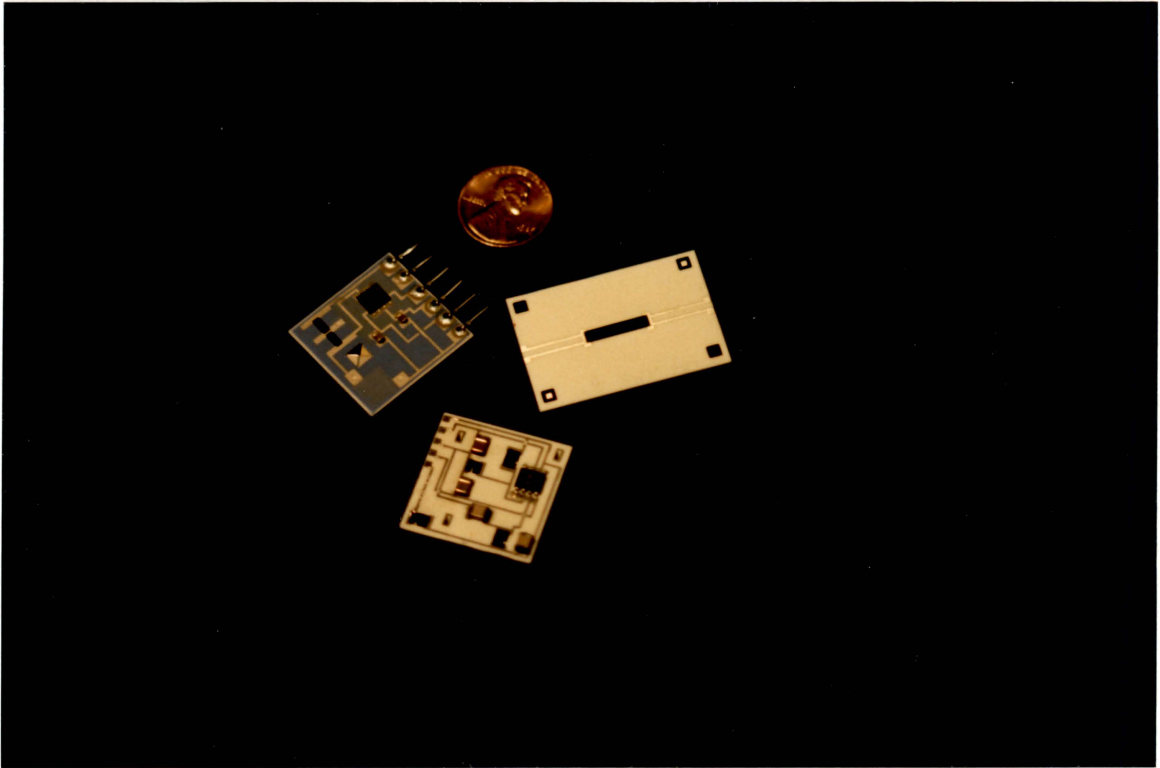

Figure 3. Hybrid circuits: a filter circuit, the test circuit and the filter circuit tested (clockwise from left)

contours without the emissivity profile. The thermal conductivity, availability, and machinability of several insulation materials were considered in choosing an insulator.

The best insulation for insertion between the circuit and the stage was determined to be Plexiglas [1]. It was readily available and easy to machine. Plexiglas is isotropic and its thermal conductivity is well defined. Teflon was not chosen because it is expensive. Phenolic materials were not chosen because of the problems associated with machining glass fibers and the uncertainty and variability of the thermal conductivity.

Despite the desirability of using the insulation, the emissivity correction used by the thermal imaging system prohibited its application. The emissivity correction procedure of the imager (Barnes Manual) requires the unpowered circuit to be heated to two different temperatures at least 30°C apart and higher than 40°C . After one radiance scan is made at each of these two temperatures the emissivity of each point or "pixel" location is computed using the formula:

$$\varepsilon = \frac{(N_{m1} - N_{m2})}{(N_{t1} - N_{t2})}$$

which is based on the assumption of an unchanging ambient temperature (Shepherd, 1987a). During the emissivity correction procedure, the radiance, N_m, is measured at each pixel and N_t , the radiance of a blackbody at the chosen temperature, is looked up in a stored table by the program. The temperature distribution of the powered circuit is then calculated by obtaining a radiance scan from which the temperature is computed using the previously evaluated emissivity.

---

1 "Plexiglas" is a registered trademark of the Rohm and Haas Company

The unpowered circuit is brought to equilibrium at two temperatures chosen for the emissivity calculation by a thermoelectric heater. The heater is adequate for heating the Device-Under-Test (DUT) when it is a highly conductive ceramic substrate. However, the addition of insulation between the substrate and the stage increases the thermal load on the stage such that a uniform, known temperature, required for the emissivity correction procedure, cannot be achieved.

2.3 Quantifying Temperature Measurement Uncertainty

There are two temperature measurements whose uncertainties were considered in the planning of the experiment. The stage temperature, T_o , is measured using a thermocouple and the junction temperature, T_j , is measured by the RM-50 imager. The uncertainty in the T_o measurement affects the T_j value calculated by the imager. Prior planning indicated that the measurement of T_o was of paramount importance to the accuracy of the junction temperature measurement and prediction. The process used to measure T_o will first be described followed by a discussion of the accuracy of the imager measurements of T_j .

2.3.1 Stage Temperature

The Omega 881C meter monitoring a type K thermocouple in preliminary experiments had an accuracy of ± 4 °C . This was later replaced by a type J thermocouple, amplifier, millivolt meter, and ice bath combination that was accurate

to better than ±1 °C . The type J thermocouple was held to the stage by a basswood lever which had a small thermal mass and a low thermal conductivity. Early comparisons of the type J (with an ice bath reference junction) and type K thermocouples showed a 10 °C difference in measurements of the stage temperature. When thermal grease was applied to the thermocouple beads the temperature difference was reduced to 3.5°C at locations 5 mm apart on the stage. The time constants of the thermocouples were quite small. The type K thermocouple time constant was estimated to be less than 1.7 s and the type J thermocouple time constant was of the same order of magnitude. The type J thermocouple applied with thermal grease was expected to meet the T_o accuracy of at least ±1 °C suggested by the imager manufacturer (Fitzsimons, 1987). In addition, a Tektronix probe with an accuracy of ±2.5 °C was used. Table 3 lists the stage temperature recorded simultaneously by the three different instruments. Agreement is clearly within the specified accuracies.

Table 3. Stage temperature measured simultaneously with different probes

Instrument	Accuracy (°C)	Temperature (°C)
Type J thermocouple	±1	98.5
Type K thermocouple	±4	101
Tektronix probe	±2.5	98.5

However, this comparison of the type J and type K thermocouples was not repeatable. On the following day, the two thermocouples were used in the same positions; i.e., the assembly was not disassembled overnight. In this second test the type J thermocouple measured 99°C and the type K thermocouple measured 105°C . One observation that may be made from these two tests is that the type K thermocouple is consistently higher than the type J thermocouple. This may be caused by the the different mounting techniques used. The type K thermocouple was wedged between the stage and the Plexiglas insulator that clamped the hybrid to the stage. The type J thermocouple was mounted under a basswood lever 7 mm away from the type K thermocouple. The primary difference between the mounting techniques was the clamp temperature. The temperature of the Plexiglas approached 50°C while the wood lever temperature did not rise much above ambient. Thermal grease was used in mounting both of the thermocouples.

Further tests were performed to analyze a perceived thermal contact problem with the type J thermocouple. Concerns also arose over the use of the ice bath. The uninsulated container that held the ice bath was not stirred regularly, so temperature stratification probably occurred. Both poor thermal contact and ice bath stratification would cause the measured temperature to be lower than the actual stage temperature. In order to check this, the previous instrumentation was not disturbed and three type J thermocouples with twisted junctions were added to the stage and the substrate. A fourth thermocouple was introduced to monitor the temperature of the ice bath, which was now stirred regularly and insulated. These four thermocouples were connected to a Hewlett Packard (HP) 3852A data acquisition instrument which has a stated accuracy of 0.6°C when used with type J thermocouples in this temperature range. Two examples of these measurements and the temperature measurement differences are shown in Table 4 on page 37 and their

locations on the stage are shown in Figure 4 on page 38. The stage temperature does not seem to be uniform.

Table 4. Stage temperature measured simultaneously with different thermocouple systems

T.C. #	Type	Instrument	Accuracy (°C)	Location	"67°C" Temperature	"99°C" Temperature
1	J	HP	±0.6	Resistor	67.1	97.6
2	J	HP	±0.6	Alumina	67.9	98.9
3	J	HP	±0.6	Stage	66.7	95.7
4	J	Fluke	±1	Stage	68	99
5	K	Omega	±4	Stage	70	103

2.3.2 Junction Temperature

The uncertainty of the junction temperature measured by the imager depends on the correct operation of the imager as well as the temperature and emissivities being measured (Table 5). The mounting of the circuit to the heater stage is critical. A thin, even coating of thermal grease should be applied between the substrate and the heater stage. Any wires connected to the circuit must be secured to the stage in order to prevent motion of the device relative to the stage during imager operation. If the device moves during a temperature measurement sequence, then the data

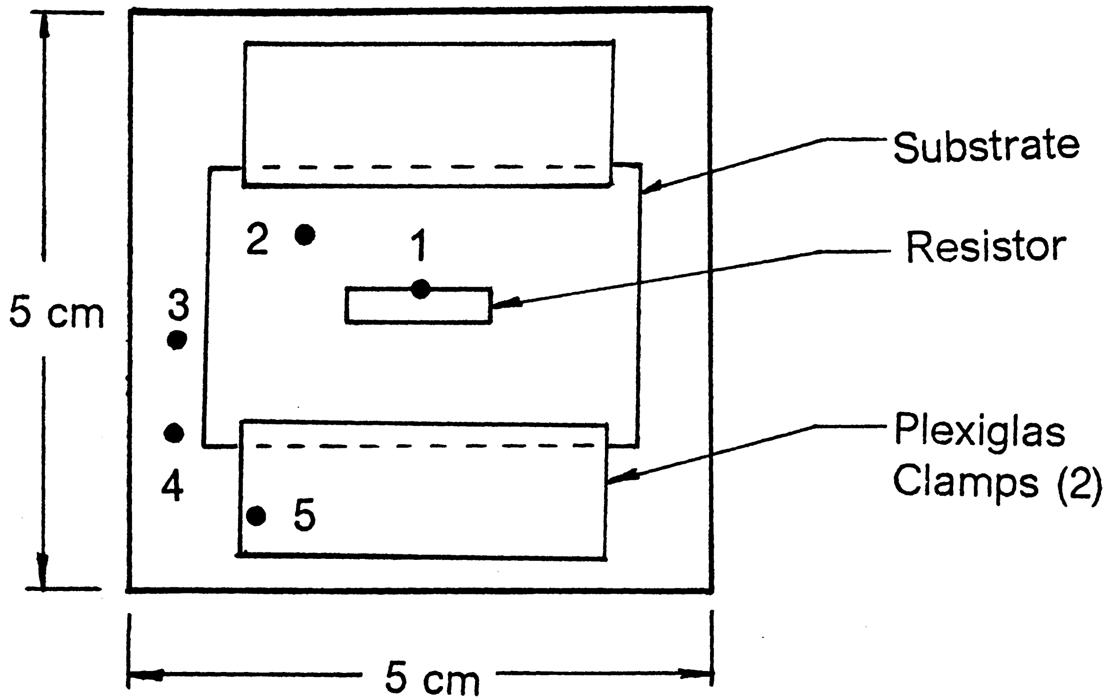

Figure 4. Thermocouple locations for the measurement of the heater stage temperature

must be discarded and the test repeated. Once the device is secure on the stage, a transition region between two materials with widely different emissivities, such as the edge of the black resistor paste where it borders the silver conductor, is brought into optical focus. The infrared detector is then focused using the black level, the span control, and the stage's vertical adjustment. Changes in the A-trace, a display of radiance verses X position on the circuit, is monitored on the imager's oscilloscope. When the detector is properly focused, the A-trace will be vertical at the intersection of two materials with different emissivities because of the variation in radiance. Poor executions of these procedures will introduce greater uncertainties into the measurement of T_j.

Table 5. Accuracy of the Barnes Engineering RM-50 Imager with CompuTherm software (Fitzsimons, 1987).

Emissivity (ε)	Accuracy (°C)
> 0.5	± 0.5
$0.25 - 0.5$	± 1.0
< 0.25	± 2.5

Uncertainty in the stage temperature measured is ± 1.0°C . Experimental conditions included free convection to the atmosphere with no large radiation sources in the substrate's field of view. Thermal grease was applied between the stage and the substrate.

The thermoelectric stage heater is limited in its ability to heat circuits to a uniform, constant temperature. The heater, with no thermal load, can provide stage temperatures of 1° – 100°C above ambient temperature in 1°C increments. The heater controller has been modified to provide temperatures above the original design range of 0° – 50°C . The stage must be maintained at a uniform, known temperature in order for the emissivity calculations to be accurate. The emissivity of one small IC package or a simple hybrid with few components can be calculated accurately. If the transient response of the specimen assembled to the heater stage is too slow to be heated uniformly, then the emissivity correction procedure will be less accurate. Circuits with many components, connectors or heat sinks will exceed the capacity of the existing heater, in which case a larger heater or an alternate method of measuring emissivity will be required.

The second set of factors affecting the accuracy of the temperature measurements is machine dependent. The temperature resolution of the imager is 0.1°C , meaning the instrument can distinguish differences in temperature of 0.1°C for temperatures near 70°C . The accuracy of the temperature measurement depends on the spatial resolution of the imager, the optical clarity over the entire field-of-view, and the uncertainties of the measurement of radiance and the calculation of emissivity. Each of these will now be discussed, followed by a summary of the uncertainty of the measurement of T_j in hybrids.

The imager is able to resolve physical features on the scanned surface as small as 15 microns, see Figure 14 in Appendix E. This resolution requires a 100X lens with its maximum field-of-view (FOV) of 1.6 mm x 1.6 mm. This FOV is well suited for examination of individual devices on a component. The measurement of temperatures over an entire hybrid or a significant portion of a hybrid is best accomplished with the 3X adjustable lens and the 10X fixed lens, respectively. The

temperature distribution over a single 3 mm x 13 mm thick-film resistor was accomplished with the 3X lens and a 18 mm x 18 mm FOV. The analysis of a 3 mm x 3 mm portion of this same resistor and the attached conductor was done using a 6.4 mm x 6.4 mm FOV.

Some anomalies associated with the optics of the imager were observed with the 10X lens but not with the 3X lens. When the mechanical zoom adjustment was set to its minimum magnification, the scan of the radiance over the resistor area showed discontinuities near the edge of the FOV, see Figure 5 on page 42. These radiance values varied by one or two color steps when a reasonable display span was chosen, even though the surface measured is flat and the material properties are constant throughout the FOV. These discontinuities are also present in the emissivity data, see Figure 6 on page 43. Minimum, maximum, and average radiances were calculated in the area away from the edge effects and then in the edge-effect region. A 7 percent difference in the two minimum values was calculated. The emissivity of the resistor paste is not expected to vary this much over the FOV. The disparities in the emissivity may result from the optics "seeing themselves" (Narcissus effect). Regardless of the problem's source, it seems to be self-correcting in the temperature data, which did not exhibit this discontinuity. The radiance and emissivity maps are combined to obtain temperature contours. There are two ways to avoid the edge-effect problems in the radiance and emissivity data. The first one is to increase the mechanical zoom, which appeared to alleviate the problem. The other is to center the DUT in a larger FOV and ignore the data near the edges.

The accuracy of the emissivity data calculated by the imager is difficult to quantify. The emissivity of the resistor paste used was not available in the manufacturer specifications. The resistor paste emissivity was estimated to be 0.95. The emissivity measured for the silver is in the 0.06 range which is three times

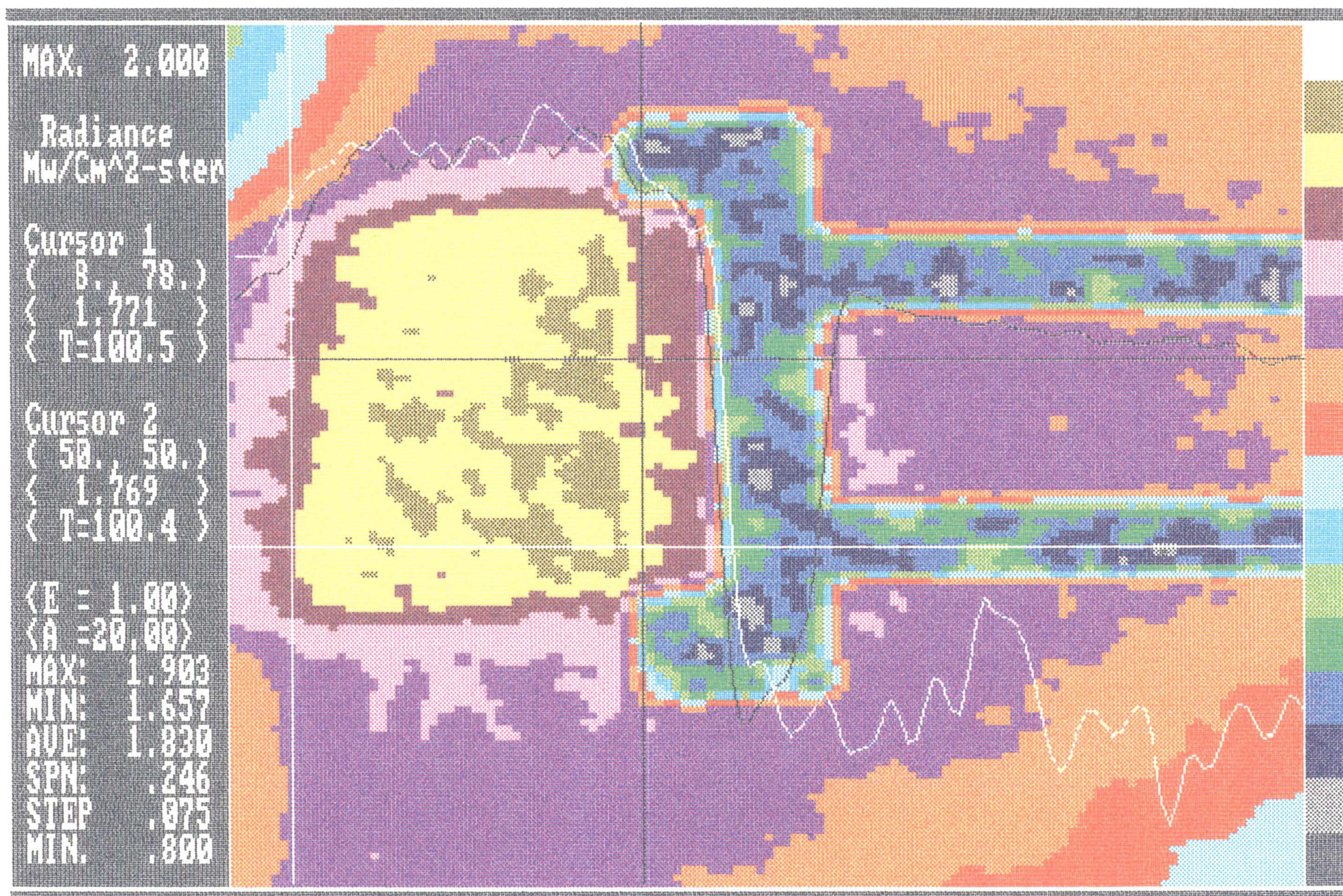

(Image size approximately 0.6 cm square)

Figure 5. Radiance scan of the unpowered test circuit with powder applied

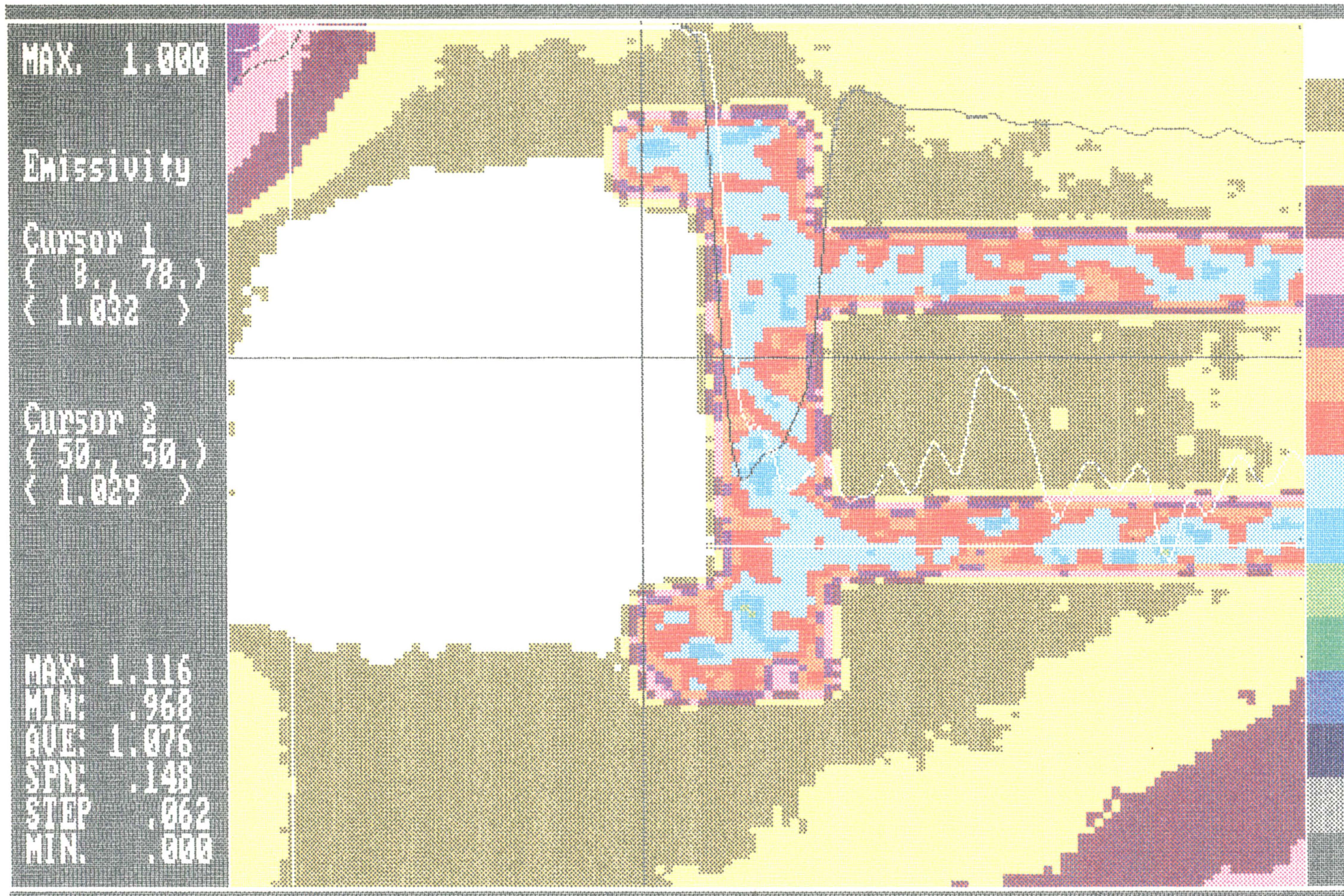

(Image size approximately 0.6 cm square)

Figure 6. Emissivity calculated for the unpowered test circuit with powder applied

greater than the 0.02 value from Siegel and Howell (1981) for polished silver. The silver conductors tested had probably oxidized, which would result in a higher emissivity value. Alumina's emissivity is given as 0.5 by Rohsenow and Hartnett (1973), while it was measured in the range of 0.56 to 0.69, a difference of 12 percent to 38 percent. These two comparisons show the disparity between published and measured values for low emissivities. The uncertainty for higher emissivities is estimated to be 10 percent. Table 6 shows the emissivity values measured and the corresponding handbook values.

Table 6. Test circuit emissivities (average values)

Material	Emissivity Measured	Emissivity From Source Cited	Source
Alumina	0.63	0.5	Rohsenow and Hartnett, (1973)
Resistor Paste	0.99	0.95	Estimated by author
Silver	0.06	0.02	Siegel and Howell, (1981)
Foot powder	0.94	0.95	Fitzsimons, (1987)

The accuracy of the radiance measurements could not be quantified because alternate measurement techniques were not available. Assuming the manufacturer's claimed temperature of ± 0.5°C, for the temperature measurement to be correct, the

radiance can be expected to be of a similar accuracy. The measurement of a very low radiance (0.1-0.2 mW/cm^2-sr) was accomplished for a powered hybrid with $T_0 = 25°C$. In this range the imager has a resolution of less than 0.01 mW/cm^2-sr . The accuracy is therefore estimated to be 0.05 mW/cm^2-sr .

The uncertainty of the temperature measurement is a function of the spatial resolution, the optical clarity, the uncertainty of the radiance measurement and the uncertainty of the calculated emissivity. The systematic uncertainty of high-temperature, high-emissivity surface temperature measurements is estimated to be 1°C . This uncertainty is computed from the difference between the random uncertainty of $\pm 1°C$ and a 2°C difference between the imager measurement and a simultaneous thermocouple measurement of a high-temperature, high-emissivity surface. The thermocouple measurement was actually 3°C lower than the imager measurement, but 1°C is accredited to the thermal contact loss. The systematic uncertainty occurs consistently throughout the measurements and could be calibrated out. The 1°C random uncertainty is the measurement accuracy referred to elsewhere in this thesis. Areas of the device with low emissivities have higher temperature measurement uncertainties because less radiation is emitted from these areas than from high emissivity areas even though both are at the same temperature. This is because less radiant energy reaches the infrared detector and therefore the signal-to-noise ratio is poorer. For the same reason higher operating temperatures reduce the measurement uncertainty because more radiant energy is emitted in the sensitive range of the IR detector.

2.4 Results

The uncertainties of measurements made are summarized in Table 7. These values are estimates based on the assumptions explained in the previous sections of this chapter.

Table 7. **Experimental Uncertainty**

Parameter	Uncertainty	Units	Type	Comments
Emissivity, ε	10	%	Systematic	
Radiance, N	0.5	$\frac{mW}{cm^2-sr}$	Systematic	
Stage Temp. T_o	3	°C	Systematically Low	Using ±0.5°C T.C. Thermal Contact Dependent
Junction Temp. T_j	1 ±1	°C °C	Systematic Random	For temps. > 100°C and $\varepsilon > 0.9$ Increases significantly for decrease in ε or for lower temp. range

Chapter 3

Experimental Equipment and Procedure

3.1 Design of Experiment

A hybrid test circuit to be studied with the IR thermal imager was designed and fabricated. A simple, one-resistor circuit was designed so that thermal interaction between multiple devices would be avoided. Doing the first measurements on a simple circuit permitted the study to focus on instrument use and experimental technique, before complex heat transfer phenomena were addressed. Follow-up studies will investigate more complex hybrid circuits. The experiments were planned while the UNCER software was being developed. The software models indicated that the uncertainty in the stage temperature measurement was critical; therefore, it was measured very carefully.

The experiments were performed to answer five questions about temperature measurements of hybrid circuits using an infrared thermal imager. These five questions consider:

1) Repeatability of data
2) Emissivity coating
3) Increased convection
4) Decreased convection
5) Rise in T_j for various T_o and voltage inputs

The measurement repeatability was tested by repeating the same experiment on two different days. Another study was undertaken to see if foot powder is an effective emissivity coating and whether or not it should be considered for use in future temperature measurements. The magnitude of the convection heat loss from the circuit was studied using two different methods. The first was to increase the convective heat transfer by introducing forced convection. This was accomplished by placing a portable fan next to the test circuit. The second convection change was affected by placing a curtain around the measurement stage. The curtain reduced the convection and radiation cooling from the circuit to the surroundings by blocking the airflow and radiation interaction. The final question studied was the relationship between the power input to the resistor and the increase in junction temperature above the stage temperature over a variety of stage temperatures and power inputs. In addition, the calibration of the imager was checked because CompuTherm calculated emissivities greater than one. The calibration check showed only a small error in the imager's temperature measurements. Finally, the temperature distribution of an operating hybridized filter circuit was measured as an example of the imager's capabilities.

3.2 *Implementation of Experiment*

3.2.1 Overview

A series of experiments was performed on a single-resistor test circuit using an IR thermal imager to measure the surface temperature of the circuit for a variety of operating conditions. Conditions varied include airflow, emissivity coating, temperature and electrical inputs. The experiments are described in three sections: the materials used, the procedures used and the method for observing and interpreting the data.

3.2.2 Materials and Equipment Used

The experiments employed an RM-50 infrared micro imager built by the Barnes Engineering Division of the EDO Corporation. The imager was supplied with a modified IBM PC and version 2.2 of the associated CompuTherm software ; the system specifications are listed in Figure 14 on page 119. The test circuit measured with this imager had one 12.5 mm x 2.5 mm resistor screen printed onto a 25.4 mm x 3.81 mm x 0.064 mm alumina (96 percent) substrate, see Figure 3 on page 32. This circuit was placed on a 75 μ-thick layer of Thermalloy Thermacote #250 thermal grease applied to a thermoelectric heater stage. The stage allowed heating to as high as 125°C with a modified Midland Ross controller. The controller provides a constant temperature, with variations of less than 1°C , (in the absence of forced

convection). At high temperatures it was found to be more difficult to adjust and maintain at a constant temperature than at low temperatures.

A set of thermocouples was used to measure the heater stage temperature during the course of the imaging experiments. The first one was a 36-gauge type K thermocouple connected to an Omega 881C meter. Subsequent temperature measurements were made with 24-gauge type J thermocouples connected to either an Omega Omni IIA amplifier, millivolt meter, and ice bath combination or an HP 3852A data acquisition instrument. Some of the temperature measurements were checked with a calibrated Tektronix temperature probe and DM502A meter. All thermocouples were applied using thermal grease. Some type J thermocouples were held in position with a wood dowel or basswood clamps whittled from dry lumber. Others were wedged under the Plexiglas clamp which holds the hybrid in place. Air velocities were measured with a TSI model 1650 meter.

3.2.3 Procedure

After the circuits were fabricated in the hybrid microelectronics lab, the thickness of the resistor paste thickness was measured and found to be 5-15 μ. The 20 circuits were then visually inspected under a microscope. Those that had dust and dirt particles in the resistor area were rejected in order to avoid discontinuities in temperature that might occur from a nonuniform resistor cross-section. A change in resistance over the cross-section due to impurities was expected to raise the resistance and therefore change the resistor temperature at the discontinuity.

3.2.3.1 Phase I

After the hybrids were inspected, the first of four experimental phases began. In this phase a series of bench top experiments was performed using two type K thermocouples, a power supply and a voltmeter. Voltages from 5V to 40V were applied to the resistor; the resistor temperature change occurred quickly. A temperature rise of 37°C occurred in 30 min for 40V when the test circuit was mounted on plywood. The initial rate of temperature increase was quick and the rate decreased as the temperature neared steady state. This phase lasted slightly more than one week.

3.2.3.2 Phase II

The acquisition of the imager by the Virginia Tech hybrid microelectronics lab marked the beginning of Phase II. The instrument was uncrated, setup and tested, then temporary clamps were assembled to hold the test circuit to the heater stage. One day was spent designing a pair of adjustable clamps to hold various size hybrids to the heater stage. The clamps permit various thicknesses of Plexiglas to be inserted between the specimen and the heater stage. A test of the thermoelectric heater's capabilities indicated that it would produce stage temperatures of 100°C above ambient. The imager was configured with the 10X lens and set to a minimum zoom. The thermal imager has two sets of optics, one for visible light and one for infrared wavelengths. Initially the circuit was optically focussed, but incorrectly focussed for the IR detector. This led to rounded corners in the IR-scanner display of the resistor-conductor interface on the circuit. A variety of stage temperatures imposed

on the bottom of the substrate and circuit voltages of 20 and 40 V gave a range of different surface temperatures. These data will be used for planning future test circuits. The time required for the substrate to reach an equilibrium temperature was also observed; specific measurements were not made, but the temperature rise for 40V seemed to take 3 min to reach equilibrium.

3.2.3.3 Phase III

Phase III of the temperature measurements began after the completion of formal training by a representative of the EDO Corporation. During, this training it became apparent that the stated accuracy of $\pm 4°C$ for the 881C meter was inadequate. Therefore, a type J thermocouple using an ice bath reference junction was substituted to measure T_o to an improved accuracy of $\pm 1°C$. This substantially improved the accuracy of the the T_j measurements obtained with the imager.

In order to minimize the temperature gradients between the substrate and the stage, thermal grease and clamps were applied to increase the thermal conductance. The substrate was placed over a thin (75 -120 μ) layer of thermal grease which covered > 60 percent of the backside of the substrate. Adjustable clamps were used to force the substrate against the heater surface. The 10X lens was installed and focussed optically first, then the vertical height was adjusted to focus the IR detector. At this point the stage was shimmed to prevent motion and misalignment between scans. Before imager operation, liquid nitrogen was added to cool the detector according to the operating instruction manual; i.e., none was spilled out of the imager's dewar, and a 30 minute warm-up time was provided for the imager (which operated without the cooling fan to minimize vibrations).

The most troublesome aspect of the measurement in Phase III was that of measuring the stage temperature. Type J and type K thermocouples were both used to measure the laboratory air temperature. For this application they agreed to within 1°C . Simultaneous thermocouple measurements seemed to show variations in temperature across the stage. The details of these measurements are discussed in Section 2.3.

The first configuration for the imager in Phase III used the 10X lens with minimum zoom. The resulting field-of-view (FOV) was 6 mm square. A radiance of the resistor-conductor transition region using this configuration is shown in Figure 5 on page 42. During all Phase III experiments the substrate was clamped securely. The type J thermocouple was positioned on the stage 5 mm from one of the short edges of the substrate.

The emissivity correction procedure must be used before the temperature can be measured. This procedure began when the unpowered circuit was heated to the low temperature, T1, and the radiance was measured and stored. Next, the circuit was heated to the high temperature, T2, and the radiance was measured and stored once again. The high temperature, T2, was also used for the Device-Under-Test (DUT) reference scan which was used to measure the ambient radiance for use in the emissivity calculation. The difference between T1 and T2 had to be at least 30°C and T1 had to be above 40°C . For the measurement of T_j in the 100°C range, these tests used T1 = 70°C and T2 = 100°C . Both of these radiance scans were stored on the diskette and the emissivity was subsequently calculated. The circuit was then powered with 40 V, the maximum voltage readily available, and allowed to reach thermal equilibrium. Once again the radiance was scanned and stored. Finally, the temperature of the powered substrate was calculated and stored.

Emissivity and temperature data arrays were stored on diskettes even though they could be recreated from the radiance data already stored. This was done because the time to reload the radiance arrays, recompute the emissivity, and then recalculate the temperature was much longer than the time to save the original data. In the same afternoon two more voltages, 100 and 150 V, were applied to the resistor and the temperature distributions were calculated based on the same emissivity data.

The second experiment of Phase III introduced forced convection over the surface of the resistor. The fan's airflow was adjusted by obstructing the flow in order to reduce the velocity of the flow to 0.2 - 0.3 m/s at 5 mm above the center of the resistor. The flow velocity was measured with a hot wire anemometer. This velocity was chosen to simulate the highest air velocity produced by the air-conditioning in the laboratory. Once again the T1/T2/ε routine was followed and the surface temperature of the resistor was measured.

The following day an additional set of Phase III measurements was made. Temperature contour measurements of the circuit powered to 40V were repeated without the fan to measure the day-to-day repeatability. After this a dark blue towel, with a heavy nap, was taped over the imager as an isolating curtain. The towel did not touch the imager stage. The towel was secured with duct tape to the imager and the table top. Care was taken to eliminate gaps in the curtain which would allow radiation or air from the room to reach the stage. Temperature contours were measured under these conditions with stage temperatures and voltages matching those used previously so that the data could be compared. The installation of the curtain caused the air temperature to rise near the substrate, but this was compensated for by the CompuTherm software and is discussed in Chapter 5.

One additional test was made before the lens was changed. A thin coating of Dr. Scholl's aerosol foot powder was sprayed over the entire hybrid test circuit as an

emissivity coating. With the stage mounted to the imager it was difficult to apply a uniform coating. Future coatings should be applied with the stage removed. The goal of coating the surface was to change the emissivity without significantly reducing the radiation or convection heat transfer mechanisms. An emissivity of 0.93-0.97 was expected based on Fitzsimon's (1987) estimate. The powder applied was estimated to be 75 μ -thick and it appeared to be uniformly distributed. The black resistor paste outline was still distinguishable through the power, but the silver conductors were not. After the powder was applied the curtain was reinstalled and the temperature was measured.

The last set of data was taken using using the 3X lens to provide a 18 mm square field-of-view (FOV) so that the entire resistor and some of the surrounding substrate could be scanned. In order to achieve this FOV the heater stage had to be clamped to a vertical work surface about 0.3 m from the imager. Once again the resistor was focussed for visible and infrared wavelengths, the temperature contours of the circuit were measured. These are shown in Figure 11 on page 92.

3.2.3.4 Phase IV

Because an emissivity of greater than unity was calculated for the single-resistor circuit by the CompuTherm software, it was necessary to determine the reason. The discrepancy between temperatures measured by the type J and type K thermocouples was considered a likely culprit. The introduction of the HP 3852A data acquisition instrument marked the beginning of Phase IV. This instrument measures temperatures to $\pm 0.6°C$ using type J thermocouples. Five type J thermocouples, two meters long, were cut from the same spool of wire as the previously used type J thermocouple. These five type J thermocouples and an

additional type K were immersed in an ice bath as a calibration check. The type K thermocouple measured 0.0°C and the 5 type J thermocouple measurements fell within the 0.11 – 0.34°C range, indicating good uniformity. A similar check of the ambient air temperatures produced six measurements within the 1°C range. While the test does not ensure similar accuracy in the 50 – 100°C range for the stage temperature, it does instill confidence in the uniformity of the thermocouples used.

Three of the five type J thermocouples were then mounted to the test circuit and the stage using thermal grease and wood lever-clamps. The purpose of the measurements was to ascertain the influence of the T_o measurement on the calculated emissivity. These temperature contours of the circuit powered to 40V were again obtained for the no-curtain, no-fan, no-powder condition. In Phase IV, 10-15 min were allowed for the circuits to reach thermal equilibrium before each radiance measurement; in contrast to the 2-5 min allowed in Phase III. If the top surface of the substrate was not at an equilibrium temperature, then the emissivity procedure would calculate incorrect values (Shepherd, 1987b).

The second most likely source of the emissivity error was an uncalibrated infrared detector in the thermal imager. To check this, two blackbody measurements were done. First a piece of cardboard was placed over the IR lens to produce a blackbody at room temperature. This radiance value was compared to the expected blackbody radiance and the corresponding temperature was 1°C higher than the room temperature measured by the 881C meter with a type K thermocouple. The second calibration test was done at 86°C using a blackbody source. The imager measured the source temperature to be 0.5°C higher than did the thermocouple connected to the HP instrument. Within the accuracy of these thermocouples, it can be concluded that the imager is within the manufacturer-specified calibration tolerances, see Table 5 on page 39.

In addition to the measurements of the single-resistor test circuit, temperature contours were also measured for a second-order low pass filter circuit containing four thick film resistors, four chip capacitors and an Analog Devices 741C op-amp on a 2.5 cm x 2.5 cm alumina substrate. The filter was then powered by +12 V DC, -12 V DC and 1 V peak-to-peak sinusoidal inputs. The filter output was shorted to ground to increase the temperature of the op-amp.

The final experiment in Phase IV was a remeasurement of the circuit emissivity with a thicker foot powder coating than previously applied. To allow for a comparison of coated and uncoated emissivities and temperatures only half the of the circuit was coated with powder. The boundary between the coated and uncoated regions ran lengthwise near the center of the resistor. The powder thickness varied from 0.25-0.64 mm. The coating was not uniform because the powder tended to make spherical clumps. The temperature was measured after 40.5 V were applied to the 1726 Ω resistor. A screwdriver blade was introduced in front of the circuit near the uncoated side of the resistor on the uncoated half of the resistor so it would be obvious which half was uncoated during the data interpretation. The temperature of this blade was that of the ambient air because it did not make thermal contact with the hybrid.

3.3 Methods for Observation and Interpretation

The CompuTherm software accepts radiance data from the RM-50 imager and displays it in 16 colors on the graphics monitor, see Figure 5 on page 42. The emissivity and temperature values calculated for each pixel are displayed in the

same manner. In the display of the temperature, for example, the left side of the display shows the minimum and maximum limits for the temperature range as selected by the operator. The STEP value given is the range divided by 16. Each division is indicated by a unique color as shown on the right-hand side of the display. This display can be plotted in color on paper by a dedicated ink-jet plotter.

A built-in cursor may be placed at any pixel in the display and CompuTherm will give the X and Y coordinates and the display parameter; i.e., the radiance, emissivity or temperature, for that location. An analog trace of the parameter as a function of X may also be plotted for that Y location. A second cursor may also be used. When both cursors are used they form a rectangular "window" between their intersections. The maximum/minimum/average values of the display parameters in this window can be calculated. The display with both cursors, both analog traces, and the max/min/ave data is the most informative method of displaying information from the imager. Two other display variations are available. The difference between two arrays of temperature, or any other display parameter, can be calculated by CompuTherm and displayed on the screen. The same two arrays of data can also be displayed side by side on the same screen to allow a visual comparison.

Chapter 4

Thermal Computer-Aided-Design (CAD)

Thermal CAD software is used to predict the temperature of electronic circuits for two reasons. The first is that the reliability of the circuit is a function of its temperature. Temperature predictions generated by the computer can be used to predict the circuit's reliability. The second reason is that money and time can be saved by thermally modeling a circuit design on the computer before building and testing a prototype. CAD analyses compute the temperature distribution in the circuit being studied by mathematically modeling heat transfer mechanisms involved. CAD software must be carefully chosen in order to accurately predict the temperatures throughout the circuit.

In this study, two software packages were used for thermal analysis. These were chosen after careful consideration of more than 15 packages. A brief description of each package considered and the reasons for using or rejecting each package is given. Software packages not used are listed in Appendix D. This is followed by a detailed description of how the chosen software was implemented. Of

these two programs, one package is commercially available and the other was written specifically for this application. The final two sections of this chapter will describe the results of the CAD analyses and discuss their significance.

4.1 Choice of Thermal Analysis Program

The choice of software packages was based on criteria that evolved during the literature review of thermal CAD and heat transfer experimentation applied to electronic circuits. Thermal CAD software can be divided into two categories. The first category is a large one that includes both finite element and finite difference schemes for solving for nodal temperatures based on the partial differential equations (PDEs) governing the heat transfer. The second category is the lumped parameter method for solving the PDEs. Both categories require a different set of assumptions.

A finite element or finite difference model of the hybrid substrate is necessary if the isotherms are to be calculated for the entire surface. A lumped parameter computer study will not yield isotherms over the surface considered, rather it will only calculate one uniform temperature for this entire area. In the case of a resistor, the finite element or finite difference methods would provide a temperature distribution but the lumped parameter will only give one temperature for the entire resistor area. The lumped parameter method is acceptable if the area being studied is small enough to be assumed uniform in temperature. The finite difference/FEM verses the lumped parameter method decision was made at the same time packages were considered based on the criteria that were developed from the literature search. This division of the available software packages into two broad categories was one

of many decisions made in the software evaluation. The criteria used throughout the evaluation will now be described.

There were four criteria against which each software package was evaluated. These were cost, availability, the start-up learning curve, and potential for future customization. Most packages failed to meet several criteria, however, none were eliminated for cost reasons alone. Each of these criteria will now be discussed. The first criteria was the purchase price and maintenance cost of the software. Many packages were available free at the Virginia Tech computing center or were in the public domain. Other packages cost thousands of dollars and, as might be expected, these were the most powerful and flexible. The availability of packages included the software and the equipment on which to run it. Personal computers (PCs) were more difficult to access than the mainframe. Finite element programs like ABAQUS and MSC/NASTRAN were available on campus but they were avoided because of the long start-up time for new users. These are suited for thermal design of a circuit and are used to make accurate predictions of temperature and stress distributions on circuit assemblies, but they require substantial training before they can be properly implemented.

The potential for future customization was a severe test of software packages. Packages that are sold only as a executable code are limited to the analysis they were programmed to perform. In this study of the accuracy of thermal CAD software, it was desirable to avoid restricting future work by using software with inherent limitations. All of the CAD software was compared to these criteria and Simulation Program for Integrated Circuit Electronics (SPICE) was chosen because of its advantages which included it ease of use.

Scott (1987) documents a good example of how SPICE is implemented. Once the Virginia Tech operating system commands were figured out, the first thermal

model was successfully run on SPICE in less than one day. Scott's (1987) example and the operating system commands are summarized in " SPICE Operation Instructions" on page 109. SPICE is readily available on the mainframe computer at Virginia Tech, therefore its purchase price did not need to be considered. It is considered an industry standard and future thermal models, even though complex, can be handled easily.

SPICE is a large and powerful general purpose circuit/simulation program for dc, transient, ac and Fourier analysis. Circuits may contain resistors, capacitors, inductors, mutual inductors, diodes, independent and dependent voltage and current sources, as well as elements such as semiconductors (Scott, 1987).

4.2 CAD Implementation

Both SPICE and the custom written software, UNCER, were used to predict T_j on the circuit. UNCER was written to overcome the limitations of SPICE and it estimates the uncertainty in the value of T_j it predicts. SPICE's capabilities and limitations will be described before those of UNCER, in order to explain why UNCER was written.

4.2.1 SPICE: Use and Limitations

Figure 7 on page 66 shows the model used for the SPICE thermal analyses of the hybrid. The heat generated by the dissipation of electrical power was modeled

as a current source and the temperature differences are analogous to voltages. The quantities R_d and R_v were calculated by hand from material properties and simple relations, and the R_r was estimated. The temperatures T_o and T_w were estimated based on temperature measurements made in the lab. To simplify the model, T_a was assumed to be equal to T_w. Once all of the inputs were specified, SPICE would be used to solve for the unknown, T_j.

The simple circuit-analog model is complicated by the dependence of R_r, the thermal radiation resistance on T_j. The energy radiated is proportional to a difference between two temperatures to the fourth power; i.e., $(T_j^4 - T_w^4)$. Convection and conduction, on the other hand, are proportional to the linear temperature difference. Estimates of R_r and the value of T_j are given by the solution of the simultaneous algebraic equations developed from an energy balance on the circuit. The quantities T_o, T_w, R_r, R_v, and R_d were then put into SPICE to verify UNCER. The comparison of the results from UNCER and SPICE is described in Section 4.3.

4.2.2 Assumptions

The UNCER model is based on assumptions that narrow the scope of the problem. This software solves for T_j in the circuit shown in Figure 7 on page 66 and it evaluates the uncertainty of the value of T_j predicted. Figure 8 shows this same circuit in the form used for the derivation of the UNCER equations.

The assumptions used are:

1) All three modes of heat transfer, radiation, convection and conduction, are important.

2) T_j is constrained to be $> 100\,^{\circ}C$

3) The spread angle is ignored in the conduction analysis

4) Net view factor $\overline{F}_{jw} = \varepsilon_j$

5) $T_a = T_w$

6) $T_j > T_o$

7) Resistor paste emissivity, $\varepsilon_j = 0.95 \pm 0.045$

8) Temperature, T_j, is constant across the entire resistor.

Most of these assumptions simplify the problem. However, the first assumption increases the complexity of this analysis. Radiation and convection are often ignored in similar analyses; e.g., Zimmer, (1983), Beccue, (1987), and David, (1977). For this analysis all three modes of heat transfer were considered in order to estimate the magnitude of each. Limitations of the thermal imager necessitate the second assumption. The sensitivity of the imager is greater at higher temperatures (Rucker, 1987). The test circuit measured only produced temperature rises of 20°C with low voltages (20-40 V) applied. By imposing a T_o in the range of 100°C on the back side of the substrate, the surface temperatures were brought into the sensitive range of the detector. These temperatures are also more indicative of those expected in more complex circuits of practical interest.

The spread angle is the angle from the vertical at which the heat is conducted through the thickness of the material considered. David (1977) recommends a spread angle of 26.6° , while Zimmer used 32° . In this analysis the angle was assumed to be zero in order to simplify the analysis. This simplification allows the conduction, convection, and radiation heat transfer areas to all be equal. Future studies should investigate a spread angle that will allow the model to have a conduction heat transfer area that is larger than the area for the other two modes of heat transfer.

The fourth assumption greatly simplifies prediction of the radiation thermal resistance. Setting the net view factor, $\overline{F}_{jw}$, equal to the resistor emissivity, ε_j , results from the junction being enclosed in a room with a much larger area than the

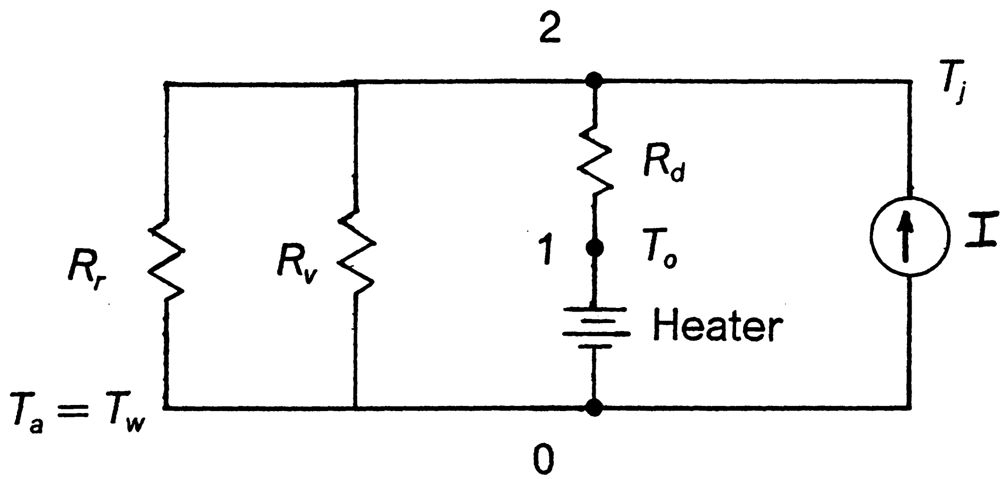

Figure 7. Electrical circuit model representing the thermal resistances (nodes numbered according to SPICE format).

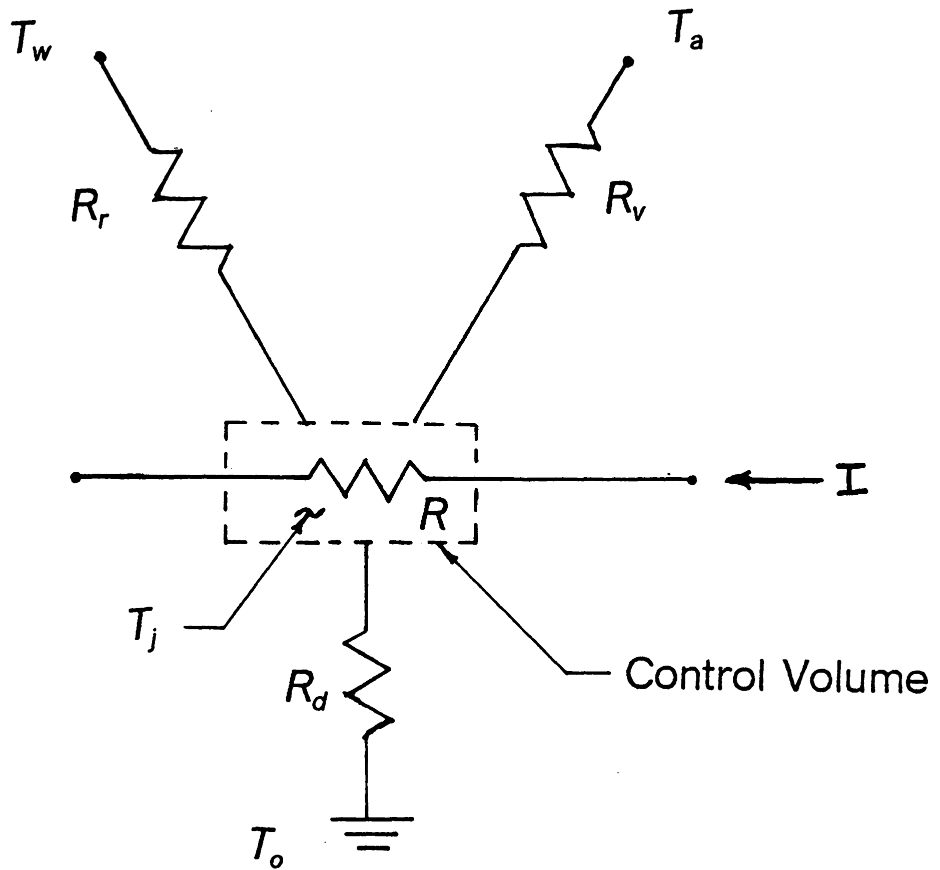

Figure 8. Thermal resistance model of the electrical circuit.

junction area; i.e., $A_w >> A_j$. For this case little radiation is reflected for the walls back to A_j , especially since A_j is not concave. Therefore, the geometric view factor between the junction and the wall, F_{jw} , is approximately equal to one. From this, it can be shown (Ellison, 1984) that the net view factor, $\bar{F}_{jw} = \varepsilon F_{jw}$, is equal to the junction emissivity, ε_j , where the heat flux is given by $Q = \sigma A_j \bar{F}_{jw}(T_j^4 - T_w^4)$. This net view factor nomenclature is consistent with that used in Ellison (1984).

The fifth assumption, $T_a = T_w$, was made because the temperature of the air in the room and the temperature of the room walls are nearly identical.

4.2.3 Derivation of Junction Temperature Equations

The junction temperature T_j of a one-resistor hybrid circuit can be estimated using the model shown in Figure 8 on page 67. For steady-state operation the heat generated by current flowing through the electrical resistor must be transmitted through the three parallel thermal resistances. An energy balance can then be written as:

$$\text{Electrical Power} = \text{Conduction} + \text{Convection} + \text{Radiation}$$

or

$$\frac{V^2}{R_e} = \frac{(T_j - T_o)}{R_d} + \frac{(T_j - T_a)}{R_v} + \frac{(T_j - T_w)}{R_r} \qquad [4.1]$$

Solving for the junction temperature gives

$$T_j = \frac{\frac{V^2}{R_e} + \frac{T_o}{R_d} + \frac{T_a}{R_v} + \frac{T_w}{R_r}}{\frac{1}{R_d} + \frac{1}{R_v} + \frac{1}{R_r}} \qquad [4.2]$$

To solve for T_j the thermal resistances must be characterized. The conduction and convection resistances are based on material properties and an estimated heat transfer coefficient.

The conduction heat transfer is described by

$$Q_d = \frac{kA}{L}(T_j - T_o) \qquad [4.3]$$

Which can be rewritten (Ellison, 1984):

$$R_d = \frac{\Delta T}{Q_d} = \frac{L}{kA} \qquad [4.4]$$

Similarly the convection heat transfer is described by

$$Q_v = hA(T_j - T_a) \qquad [4.5]$$

where

$$R_v = \frac{\Delta T}{Q_v} = \frac{1}{hA}$$ [4.6]

The radiation heat transfer is more difficult to describe because it depends on the difference of temperatures to the fourth power. It is given by

$$Q = \sigma A_j \bar{F}_{jw}(T_j^4 - T_w^4)$$ [4.7]

Introducing a new radiation heat transfer coefficient, h_r, this can be written

$$Q = h_r A_j (T_j - T_w)$$ [4.8]

This results in a thermal radiation resistance of

$$R_r = \frac{\Delta T}{Q_r} = \frac{1}{h_r A_j}$$ [4.9]

or

$$R_r = \frac{(T_j - T_w)}{\sigma A_j \bar{F}_{jw}(T_j^4 - T_w^4)}$$ [4.10]

To solve for T_j the values of T_o, T_a, T_w, h, A, k, and L must be measured or estimated. The thermal conductivity, k, of alumina is given by Dettmer and Charles (1987). The surface area, A, and the thickness, L, of the substrate were easily measured. The convective heat transfer coefficient was estimated using the relation given by Holman (1976) for laminar convection:

$$h = 1.32(\frac{\Delta T}{L})^{0.25} = 9.89 \quad W/m^2 - {}^\circ C \qquad [4.11]$$

This value of h is calculated with T_j and T_a constant at 125°C and 25°C , respectively. Future models should allow the heat transfer coefficient, h, to vary with T_j and T_a and they should verify that the flow is laminar. The ambient and stage temperatures, T_a and T_o, were measured. Equations 4.4, 4.6, 4.10, and $h = 9.89 \quad W/m^2 - {}^\circ C$ were substituted into 4.2. The measured and estimated parameters along with an iteration tolerance were input to a Newton's method root-solver to find T_j .

4.2.4 Uncertainty in Software Prediction of Junction Temperatures

The uncertainty of the predicted T_j depends on the accuracy to which each of the variables is measured or estimated. The uncertainties are combined using a method developed by Kline and McClintock (1953) that relates the uncertainty of the desired result to the uncertainties of the parameters on which the result depends.

For a result, x, that depends on y and z, the uncertainty in x is given by

$$\omega x = \pm[(\frac{\partial x}{\partial y}\omega y)^2 + (\frac{\partial x}{\partial z}\omega z)^2]^{1/2} \qquad [4.12]$$

In this investigation, T_j was a function of eight variables: T_o, T_a, T_w, V, I, R_r, R_v, and R_d. Using Eqn. 4.12, the uncertainty of T_j can be written as

$$\omega T_j = \pm[(\frac{\partial T_j}{\partial V}\omega V)^2 + (\frac{\partial T_j}{\partial I}\omega I)^2 + (\frac{\partial T_j}{\partial T_o}\omega T_o)^2 + (\frac{\partial T_j}{\partial T_a}\omega T_a)^2 + \ ....$$

$$..... \ (\frac{\partial T_j}{\partial T_w}\omega T_w)^2 + (\frac{\partial T_j}{\partial R_r}\omega R_r)^2 + (\frac{\partial T_j}{\partial R_v}\omega R_v)^2 + (\frac{\partial T_j}{\partial R_d}\omega R_d)^2]^{1/2} \qquad [4.13]$$

Equation 4.12 can also be applied to determine the uncertainties of the thermal resistances given by Eqns. 4.4, 4.6, and 4.10:

$$\omega R_r = \pm[(\frac{\partial R_r}{\partial \varepsilon_j}\omega \varepsilon_j)^2 + (\frac{\partial R_r}{\partial A_j}\omega A_j)^2 + (\frac{\partial R_r}{\partial T_o}\omega T_j)^2 + (\frac{\partial R_r}{\partial T_w}\omega T_w)^2]^{1/2} \qquad [4.14]$$

$$\omega R_d = \pm[(\frac{\partial R_d}{\partial A_j}\omega A_j)^2 + (\frac{\partial R_d}{\partial k}\omega k)^2 + (\frac{\partial R_d}{\partial L}\omega L)^2]^{1/2} \qquad [4.15]$$

$$\omega R_v = \pm[(\frac{\partial R_v}{\partial A_j}\omega A_j)^2 + (\frac{\partial R_v}{\partial h}\omega h)^2]^{1/2} \qquad [4.16]$$

The uncertainties of the measured variables; i.e., T_o, T_s, V, R_e, and L, were obtained from the appropriate measuring instrument specifications and were input to UNCER. The uncertainty in the current, I, was calculated directly from the meter sensitivities associated with the measurements of R_e and V. The uncertainty of the thermal conductivity was estimated based on a comparison of five published values.

Of the eight terms in Eqn. 4.13 only two were significant, ωT_o and ωR_d. An order of magnitude study of Eqn. 4.13 using the values in Table 8 on page 74 and $\omega T_o = 1.05$ provides these values:

$$\omega T_j \quad = \quad \pm[10^{-4} + 10^{-4} + 1.1 + 10^{-6} + 10^{-6} + 10^{-4} + 10^{-4} + 0.094]^{1/2} \qquad [4.18]$$

This order of magnitude study showed that ωT_o was the determining factor in the uncertainty of ωT_j. This variation was studied and is shown in Figure 9.

4.3 Results of Software Trials

The software prediction was improved by incorporating more exact mathematical models for each parameter used in the prediction of T_j. One change that significantly improved the performance of the software was the replacement of a crude iterative solver with a Newton's method rootfinder. The number of iterations necessary to converge to a solution for T_j within a tolerance of 0.00001 was reduced

Table 8. Input data for UNCER to calculate the uncertainty in junction temperature as a function of stage temperature.

VARIABLE	UNITS	VALUE x	UNCERTAINTY ω	RATIO $\frac{\omega}{x}$
RESISTANCE,	Ω	1762.0	9.0	0.010
VOLTAGE,	V	40.0	1.1	0.028
AMBIENT, T_a	°K	294.0	4.0	0.014
HEATER STAGE, T_o	°K	373.0	0.0 - 4.0	--
WALL TEMP, T_w	°K	294.0	4.0	0.014
H.T. AREA	cm^2	0.387	0.19	0.5
THERMAL COND	W/cm K	0.26	0.05	0.19
HYBRID THICKNESS	cm	0.064	0.013	0.2
CONV. H.T. COEF.	W/cm^2	0.0010	0.00025	0.25
EMISSIVITY	--	0.95	0.045	0.047

ITERATION TOLERANCE = 0.00001 used in T_j root finding

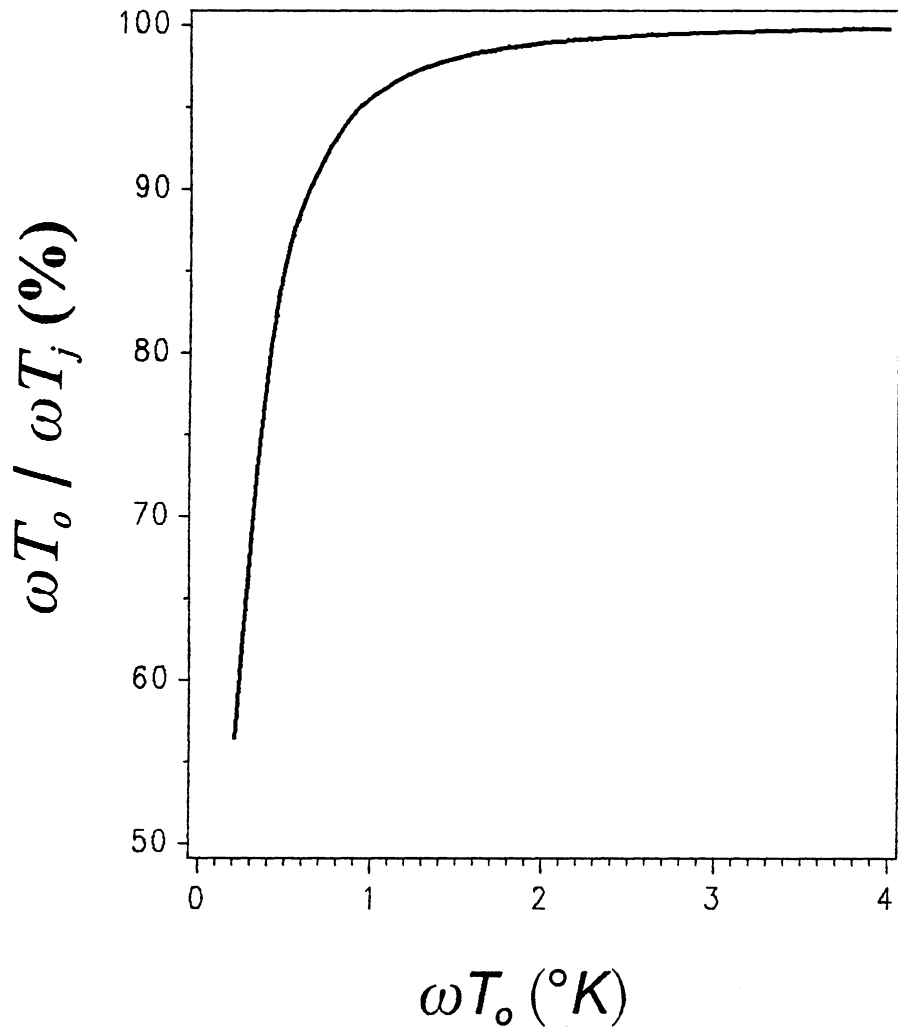

Figure 9. Percentage of uncertainty in the junction temperature attributable to uncertainty in the stage temperature.

from more than 40 iterations to less than four. An error flag was added to the program to ensure that the rootfinder located the correct root.

For the input values listed in Table 8 and $\omega T_o = 1.05°K$ the junction temperature prediction was made for a stage temperature of $T_o = 374.05°K$. UNCER calculated $T_j = 374.59°K$, which will be compared to the measurements of T_j in Chapter 5.

As a check of the values predicted by UNCER, the predicted value of T_j was compared to the value calculated by SPICE for the same model. Both programs predicted T_j to be 373.6 °K for $T_o = 100$ °C.

The current in each branch was calculated for the thermal resistance network shown in Figure 7 on page 66. These currents, shown in Table 9, represent the amount of input power leaving the circuit through each of the three modes of heat transfer. This calculation shows that most of the heat leaves the circuit via conduction. This seems reasonable for this slab of highly conductive alumina. The radiation resistance is high because the temperatures are low (on the order of 373°K) on the absolute scale. The convection resistance is high because the heat transfer coefficient is low for natural convection.

The magnitudes of these thermal resistances determine a large portion of the uncertainty in the predicted junction temperature. It might be expected that a large uncertainty in the area would cause a large ωT_j. UNCER showed this was not the case for ωA = 50 percent, as shown in Table 8 on page 74. The large uncertainty in area caused the thermal resistances to have uncertainties above 50 percent but the partial derivatives in Eqn. 4.13 of T_j with respect to each thermal resistance were more important than these 50 percent uncertainties. Large thermal resistances in the R_r and R_v terms in Eqn. 4.13 caused the partial derivatives to be small enough to cancel out the uncertainties of >50 percent. Further comparisons of these

temperature predictions and heat transfer percentages to experimental results are given in Chapter 5.

Table 9. The heat transfer into and out of the resistor.

POWER LOSS	UNITS	VALUE	PERCENTAGE OF TOTAL
TOTAL INPUT	W	0.908	100.0
POWER OUTPUT:			
CONDUCTION	W	0.837	92.2
CONVECTION	W	0.039	4.3
RADIATION	W	0.032	3.5

TOTAL OF FRACTIONS			100.0

4.4 Recommendations

The junction temperature and its uncertainty were predicted by using software based on heat transfer relations. This technique can also be used to model more complex circuits. In this manner, the uncertainty of a desired result can be reduced by improving the accuracy of the inputs which have the greatest effect on the uncertainty.

Three possible areas of future work will be discussed. One area is to study the effect of varying the effective heat transfer area on the prediction of T_j using the

UNCER software. UNCER calculated ωT_j for ωA = 50 percent, but experiments were not done to determine what size area could be assumed at a uniform temperature for a given difference between the predicted and measured temperatures. The uncertainty of the heat transfer area was significant since it was difficult to determine the portion of the circuit surface area transferring heat at the assumed uniform temperature, T_j. The area used in the heat transfer model was the area within the resistor outline. However, the temperature of the substrate outside of, but near, the resistor border is close to that of the resistor. Conduction from the resistor to the substrate creates a temperature gradient from the high temperature at the core of the resistor to the stage temperature at the edge of the hybrid circuit, as seen in Figure 10 on page 79. Therefore, it is difficult to determine the effective heat transfer area for the uniform-temperature-area model. A better value for the effective area could be determined from measurements of the circuit using the IR imager with the 3X lens. From these data the minimum, maximum, and average temperature within the resistor outline could be calculated to determine the effective area dissipating heat at the assumed temperature, T_j. One example of this technique is shown in Chapter 5; this technique should be used again.

Two more investigations could study the temperature distribution in the hybrid with more sophisticated analyses. These studies would improve on the uniform temperature assumption used in UNCER to predict more accurate junction temperatures. Chapter 5 explains the 6°C corrected difference between the measured and predicted values of T_j. This difference is large because T_j is predicted as only 0.6°C higher than the stage temperature, while the temperature measured is 6°C higher than T_o. This junction temperature prediction seems too low and should be improved.

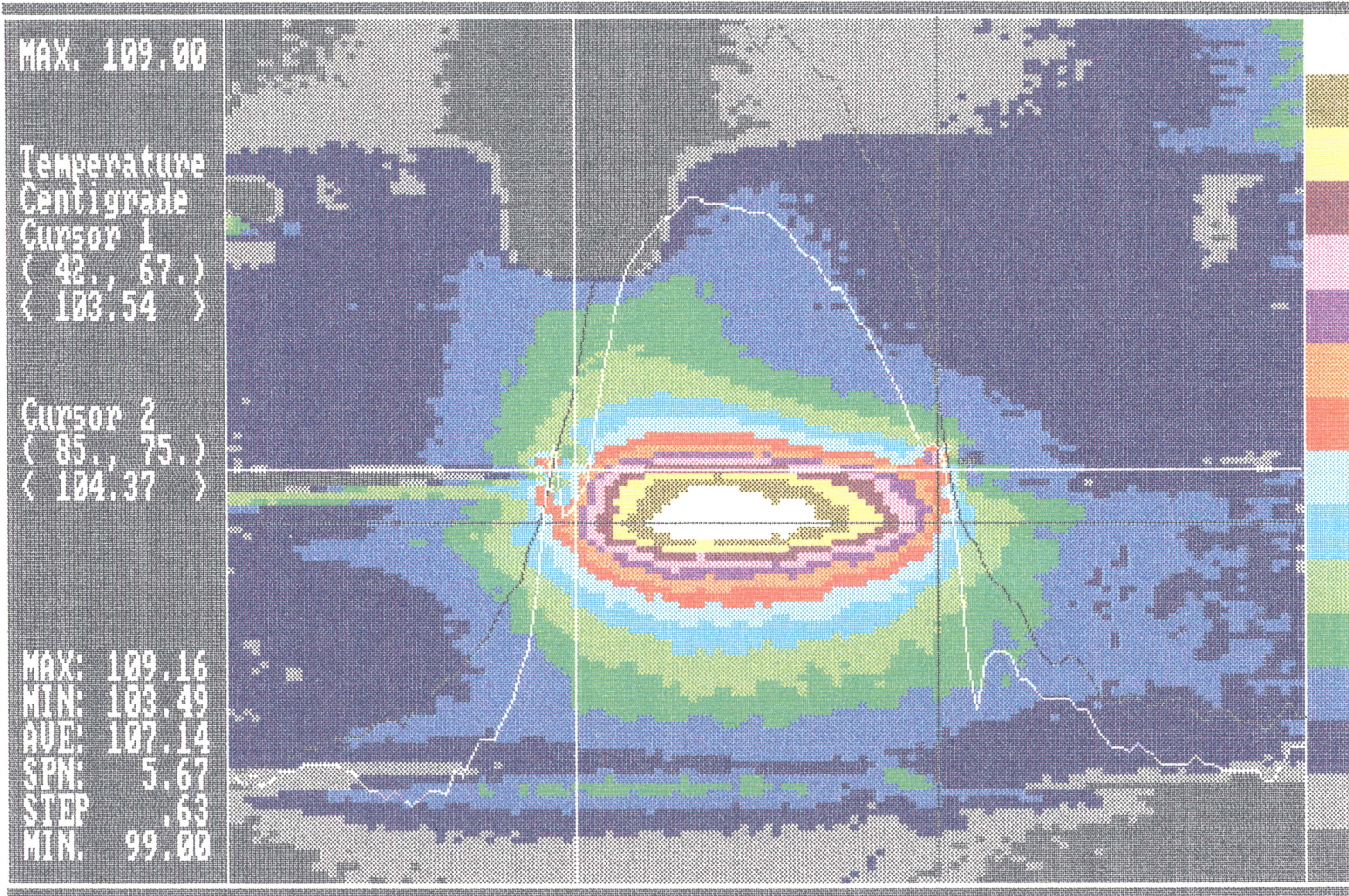

Figure 10. Temperature contours of a 1726 ohm resistor circuit powered to 40.5 volts and mounted on a 100 C stage

The imager's 1°C accuracy is sufficient to verify detailed computer studies. One investigation might build on Zimmer's (1983) use of the generator capabilities of SPICE2. His model considers temperature-dependent characteristics of devices and materials. The other investigation might follow David's (1977) use of Fourier techniques to solve Laplace's equation.

Chapter 5

Results

5.1 Experimental

This discussion of the experimental results must answer the five questions raised in Chapter 3:

1) Repeatability of data
2) Emissivity coating
3) Increased convection
4) Decreased convection
5) Rise in T_j for various T_o and voltage inputs

In addition to these results, a comparison of the predicted junction temperature and the measured temperatures is given. Temperature measurements of a filter circuit are also included as an example of the imager's capabilities with hybrid circuits.

5.1.1 Repeatability

The standard circuit heat transfer boundary conditions were chosen for testing the repeatability of the imager data. The temperature measurements were made without a fan, powder, or towel. The same emissivity and temperature measurement procedures were used on two consecutive days. The same input voltage and stage temperature were used on both days. A comparison of the data was done using a side-by-side display on the graphics terminal. Only slight variations in the isothermal regions were visible in the two displays. A CompuTherm difference calculation between these two temperature arrays indicated a maximum difference of 0.8°C , with a 0.2 – 0.4°C difference over most of the surface.

5.1.2 The Emissivity Coating

The imager inaccuracy for temperature measurements of low emissivity materials is at least 2.5°C which is worse than the 0.5°C for high emissivity materials. One solution to this problem is the application of an emissivity coating, usually a black paint, to the surface in order to increase the emissivity. The disadvantage of the black paint is the difficulty in removing it. Dr. Scholl's aerosol foot powder was tested as a coating because it has an estimated emissivity of 0.95 (Fitzsimons, 1987) and is readily removed by wiping. Typically, only trace amounts remained after a thorough wiping with cottons swabs. However, compressed air alone did not clean the surface adequately.

The foot powder was applied and tested with two different thicknesses: 0.08 and 0.6 mm. The first coating was found to be too thin because it did not raise the

Table 10. Results of emissivity coating comparisons

		Measurement Set #1			Measurement Set #2		
		Resistor Center	Alumina	Silver	Resistor Center	Alumina	Silver
No Emissivity Coating	ε	1.05	0.71	0.06	1.11 *	0.75	0.08
	$T_j - T_o$ Max. °C	7	---	---	6	---	---
Emissivity Coating	ε	0.96	0.93	0.93	1.06 *	0.87	0.50
	$T_j - T_o$ Max. °C	7	---	---	6	---	---
	Thickness	Thick			Thin		
Stage Temp.	T_o °C	100			99		
	Meter	Type J thermocouple with HP instrument			Type J thermocouple with millivolt meter		
Convection Reduction		No Convection Reduction Power Input = 0.95 W			Reduced Convection Power Input = 0.91 W		

* Average value including lower values in "edge-effect region", described in Chapter 2

emissivity of either the alumina substrate or the silver conductors above 0.9. The thicker coating increased the emissivity of the entire surface above 0.83, and most values were between 0.9 and 0.99. These results are listed in Table 10 on page 83. The temperature difference, $T_j - T_o$, is larger for cases without convection reduction than for the case with this reduction because of the increased power input to the resistor. The input voltage was nearly identical in both cases, but the second test involved a lower-resistance resistor which consequently dissipated more power. The difference between the surface and the stage temperature is not provided for the alumina and silver because identical locations for different temperature data sets could not be easily compared.

The second application of the coating was thick enough to interfere with the convection heat transfer from the surface, but this mode of heat transfer is small in the cooling of the hybrid. The temperature distribution is typically 1.5°C higher on the coated half than on the uncoated half. The coated half exhibited higher temperatures further from the center of the resistor because the coating acted as an insulator for convective cooling. It is recommended that future experiments on low emissivity surfaces should use a powder coating with a thickness of 0.6 mm or less.

The imaging system determined some emissivities to be greater than 1.0 because of uncertainties in the calculation. Chapter 2 describes the 10 percent uncertainty in CompuTherm's emissivity calculation for a properly instrumented imaging system. The resistor paste has a high emissivity, probably 0.98 or 0.99, but the imaging system determined it to be > 1.0 as seen in Table 10 on page 83. The 1.05 and 1.06 emissivities are within the 10 percent uncertainty expected from CompuTherm's calculation. However, the highest value of 1.11 is more than 10 percent above the expected value. This higher uncertainty is probably a result of the uncertainty in the stage temperature measurement. This stage temperature was

measured with a type J thermocouple using an ice bath reference junction. In Section 2.3.1 the uncertainty of this temperature measurement was given as > 3.0°C when used improperly. This uncertainty produces an uncertainty in the emissivity calculation of 13 percent which is evidenced by the data in Table 10.

5.1.3 Changes in Convection Heat Transfer

The laboratory air-conditioning system was expected to lower the junction temperature by circulating air over the test circuit and increasing the convective heat transfer. This convection was simulated by the introduction of a fan into the experimental setup. The fan lowered the junction temperature by lowering the stage temperature, because the stage was unable to supply the increased heat flux necessary to maintain a constant stage temperature. This stage temperature was expected to decrease when forced convection was introduced, and this reduced junction temperature could not be compared to the junction temperatures from other tests without forced convection. Future experiments must limit the use of the imager to rooms where airflows from air-conditioning, open doors and other sources will not effect the DUT.

Reduction of the convection and radiation heat transfer from the test circuit was expected to raise the junction temperature. Experiments measured the increase in junction temperature to determine whether or not the air currents in the laboratory would impact the junction temperature. The addition of a curtain, to reduce the convection and radiation, raised the ambient temperature by 10°C , but it did not affect the room air temperature. The decrease in convection and the subsequent rise in the ambient temperature did not significantly impact the junction temperature as

Table 11. Variations in the convection heat transfer

	Convection Increased	Convection Unchanged	Convection Reduced
T_a, °C	21.5	23	32
T_{room}, °C	21.5	23	22
Air Velocity, m/s	0.2-0.3	Not Detectable (Typical lab Conditions)	Negligible (Curtain Installed)
T_o, °C	98 *	99	99
Maximum $T_j - T_o$, °C	6	6	6
T_o Instrument	Type J thermocouple with millivolt meter		

* Operation of fan simultaneously lowers heater and hybrid temperatures

seen in Table 11 on page 86 which lists the differences between junction temperatures for three convection conditions. The difference of less than 0.5°C in the junction temperature between the natural and forced convection conditions verifies the UNCER prediction that the convection heat loss is small relative to the conduction heat transfer. In future experiments the convection heat transfer from the circuit should be monitored, but further use of the curtain is not necessary for thick-film resistor experiments because the imager can measure temperatures accurately for a known stage temperature. However, this may not be the case for components with significant height, such as SMDs, transistors and chip capacitors.

5.1.4 Variations in Input Voltages and Temperatures

The temperature rise in the thick-film resistor depends on the voltage and stage temperature applied to it. A range of voltages was applied to the test circuit at three different stage temperatures. The resulting increases in resistor temperature above the stage temperature are listed in Table 12 on page 89. Power dissipation of less than one-quarter watt over the 39 mm^2 resistor area causes very small temperature rises which are difficult to detect experimentally. Significant increases in the resistor temperature occurred when one watt or greater was dissipated by this same resistor. The dissipation of five or more watts over this same area is unreasonable for the testing of software for circuit design because practical circuit designs would not incorporate such a large power requirement. Practical circuits are manufactured with semiconductor devices which dissipate large amounts of heat and resistors that dissipate small amounts. Test circuits which use only resistors to

generate the high temperatures required for measurement accuracy should be designed so that each resistor dissipates 1-3 W.

5.1.5 Comparison of Experimental and Analytical Results

The UNCER computer heat transfer analysis predicted a uniform junction temperature of 100.6°C over the entire resistor for the values shown in Table 8 on page 74 with $\omega T_o = 1.05°C$. The measured isotherms must be averaged over the entire resistor before a comparison to the temperature value from the computer model can be made. Two methods of averaging the temperature over the resistor were used. The first used CompuTherm's averaging calculation over the area just inside the resistor limits to obtain an average temperature from three data sets. This comparison yields large differences between the predicted and measured values, so a second comparison was developed. The second comparison averaged the temperature measured over the area of the substrate heated by the resistor, which is larger than the resistor area because the alumina conducts heat from the resistor into the stage. The results of each comparison will be discussed independently.

CompuTherm's averaging feature calculated the average temperature for three measurements of the temperature distribution over most of the resistor. The distribution of isotherms in Figure 10 on page 79 is typical for the three tests. One important feature to notice is the continuity in the isotherms near the edges of the resistor, despite the change in material. However, the temperatures measured near

Table 12. Resistor temperature increase above stage temperature as a function of power dissipated by the resistor.

Stage Temperature (°C)	Voltage (volts)	Power (watts)	ΔT (Resistor to Stage) (°C)
70	20	0.227	< 1.0
70	40	0.908	4
85	40	0.908	4
100	20	0.227	1
100	40	0.908	6
100	100	5.67	40
100	150	12.7	> 80

Uncertainty in the stage temperature measured is ± 4.0 °C . Experimental conditions included free convection to the atmosphere with no large radiation sources in the substrate's field of view. Thermal grease was applied between the stage and the substrate.

the coated/uncoated interface had large discontinuities on one end of the resistor, because of the uneven line that separated the two regions. To avoid these discontinuities the cursors were positioned slightly inside the edge of the resistor for the average temperature calculation. The average temperatures of the resistor would be an estimated 0.5°C lower if these edge regions were accounted for. The average temperature increases above T_o for the resistor, excluding the edges, were measured to be 5.9°C , 6.2°C , and 6.3°C . Therefore, a reasonable estimate for the average temperature of the resistor above the stage temperature is 6.1°C . With a stage temperature of 100°C and using the estimated 0.5°C correction, the resistor temperature would be 106.6°C . The difference between the measured value and the predicted value of 6°C is attributed to the simplicity of the model.

The uniform junction temperature predicted by the model is expected to be higher than the average temperature measured within the resistor limits because heat spreading outside of the resistor boundaries is not modeled. The temperature measurements exhibit this spreading over an area approximately two times the size of the resistor. Contrary to this expectation, the first set of average temperatures calculated were consistently lower than those measured. In an attempt to relax this constraint, the temperature was also averaged over areas 200 percent and 300 percent larger than the resistor outline. The heat transfer area in the lumped-parameter model was increased by the same amount. The area was only expanded in the resistor width direction since the thermal conduction was primarily in this direction. Figure 11 on page 92 shows this spreading and the 200 percent boundaries. The results for these expanded areas and a $T_o = 98°C$ are listed in Table 13 on page 91. The difference between temperature T_j measured and temperature T_j predicted, is lower than the 6.1°C previously calculated, but the difference as a percentage of the measured $T_j - T_o$ actually increases. Therefore,

Table 13. A comparison of predicted and measured junction temperatures for To = 98 C

Resistor Area (%)	100	200	300
CompuTherm Average T_j (°C)	103.2	101.8	101.0
UNCER Prediction T_j (°C)	98.5	98.3	98.2
Difference (°C)	4.7	3.5	2.8
Percent Difference † in $(T_j - T_o)$ predicted and measured	90%	92%	93%

† $$\frac{(T_j - T_o)_{measured} - (T_j - T_o)_{predicted}}{(T_j - T_o)_{measured}} \times 100$$

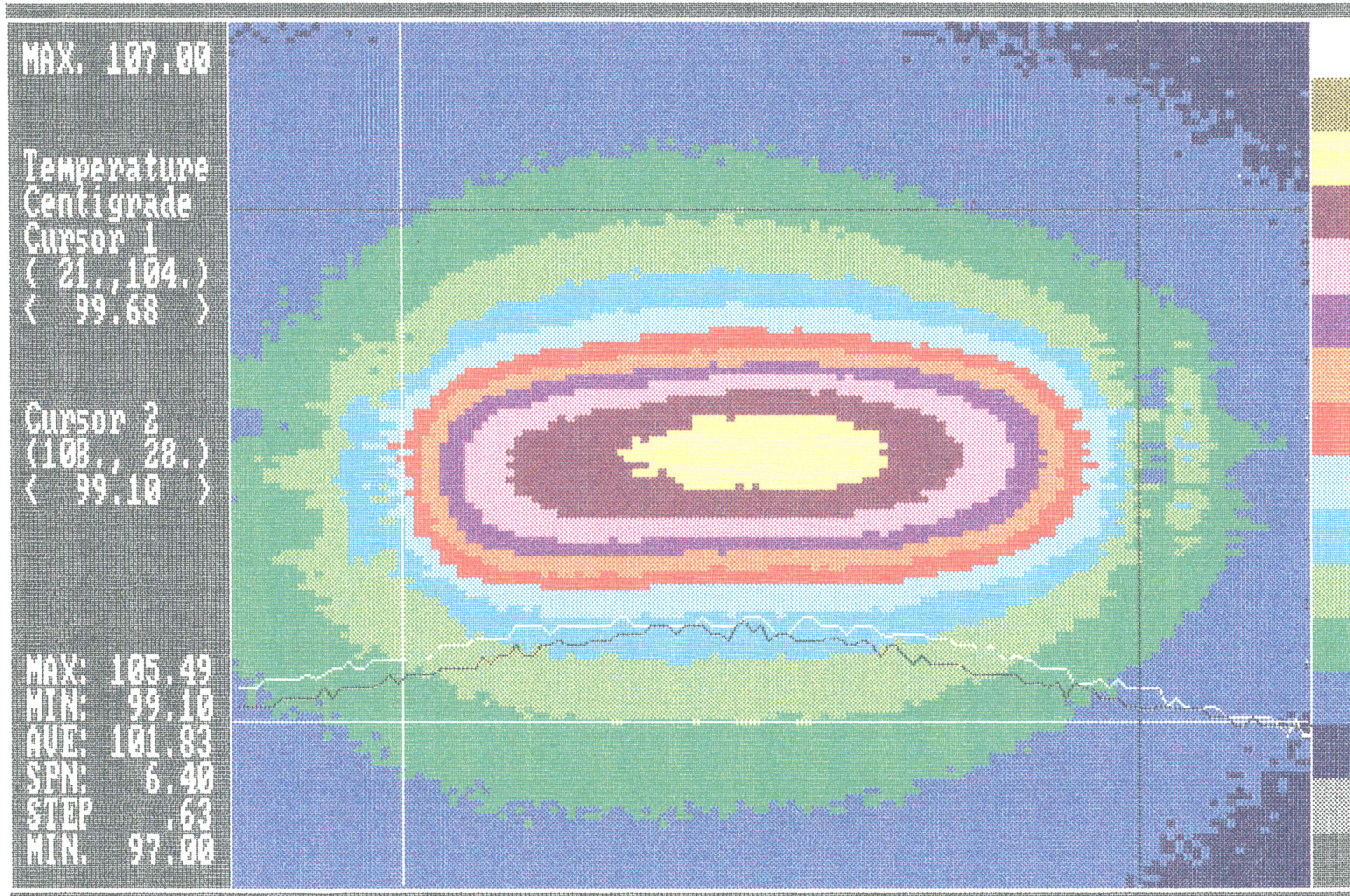

Figure 11. Temperature contours of a 1762 ohm resistor mounted on a 98 C stage

while the heat spreading area is an important parameter, it does not explain the discrepancy between the measured and predicted temperatures.

The comparisons between temperatures measured by the thermal imager and those predicted by the uniform-temperature-area model evidence the limited accuracy achievable with such a simplistic model. A more complex model will be required in order to obtain better agreement. Nonetheless, the usefulness of the imager temperature measurements for analysis verification has been demonstrated.

5.1.6 A Thermal Image of an Operating Hybrid Circuit

As an example of the IR thermal imager measurement capabilities on more complex circuits, a hybridized filter circuit was scanned. This filter, shown in Figure 3 on page 32 had one op-amp, four resistors and four capacitors. The SMD op-amp is the largest device in the circuit, and to its left are two black resistors and two brown chip capacitors. The radiance scan, Figure 12 on page 94, of the circuit at a uniform temperature shows the outline of some of the components as highlighted by emissivity differences. The black resistors have a high emissivity (approximately 0.98) so they appear as either gray or white. The op-amp is located at the white cursor intersection and the capacitors appear brown. The Plexiglas insulators that hold the substrate to the stage are areas of uniformly reduced radiance at the top and bottom of the plot. In Figure 13 on page 95 the op-amp temperature contours are most clearly visible because the temperature rises in other components are relatively much lower. Well-designed hybrids will generally contain resistors with low power dissipations relative to the active devices, such as op-amps, transistors, and other ICs. In the study of operating temperatures of a hybrid, the hot spots are of

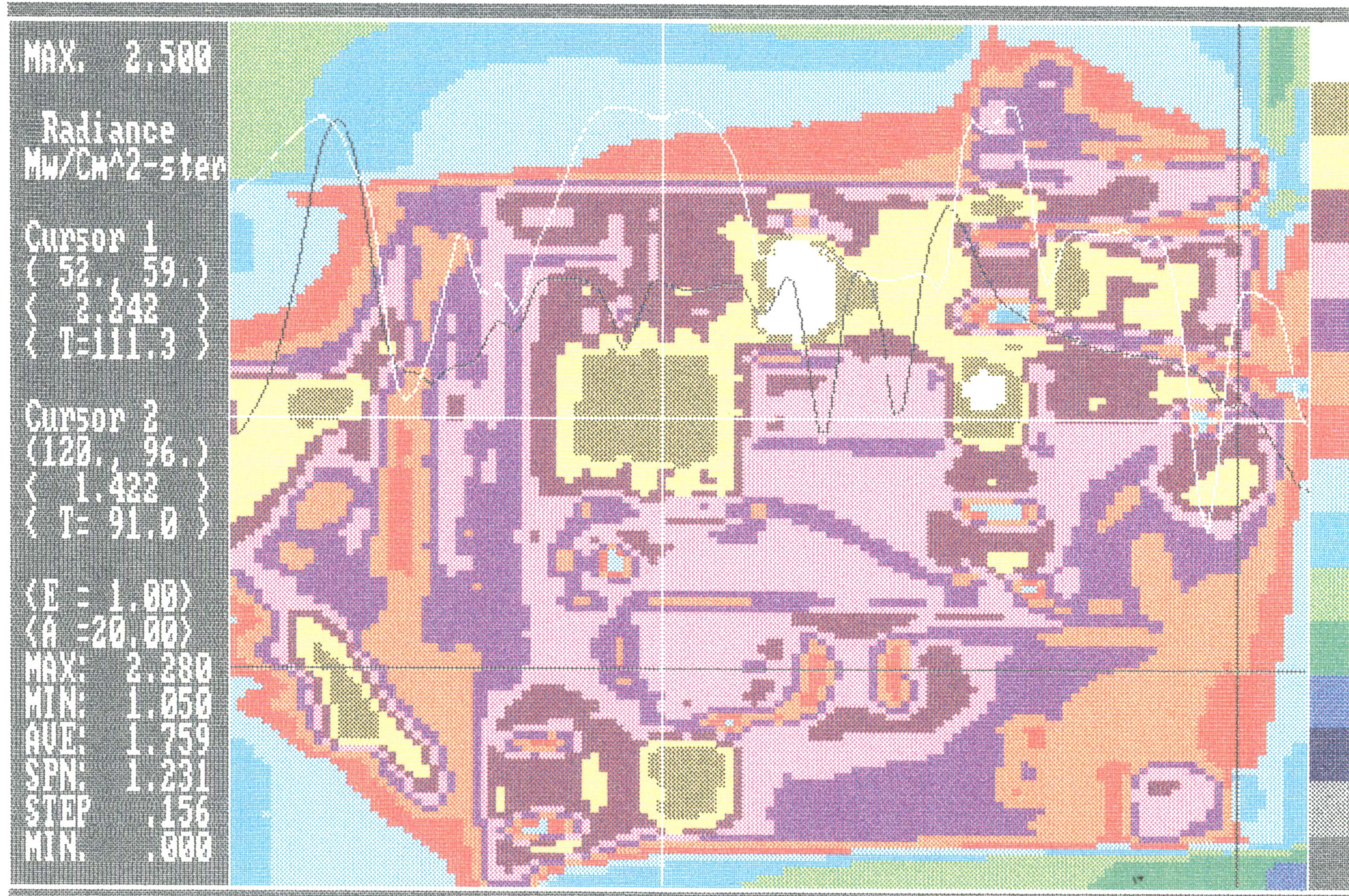

Figure 12. Radiance contours of an unpowered filter circuit mounted on a 110 C stage

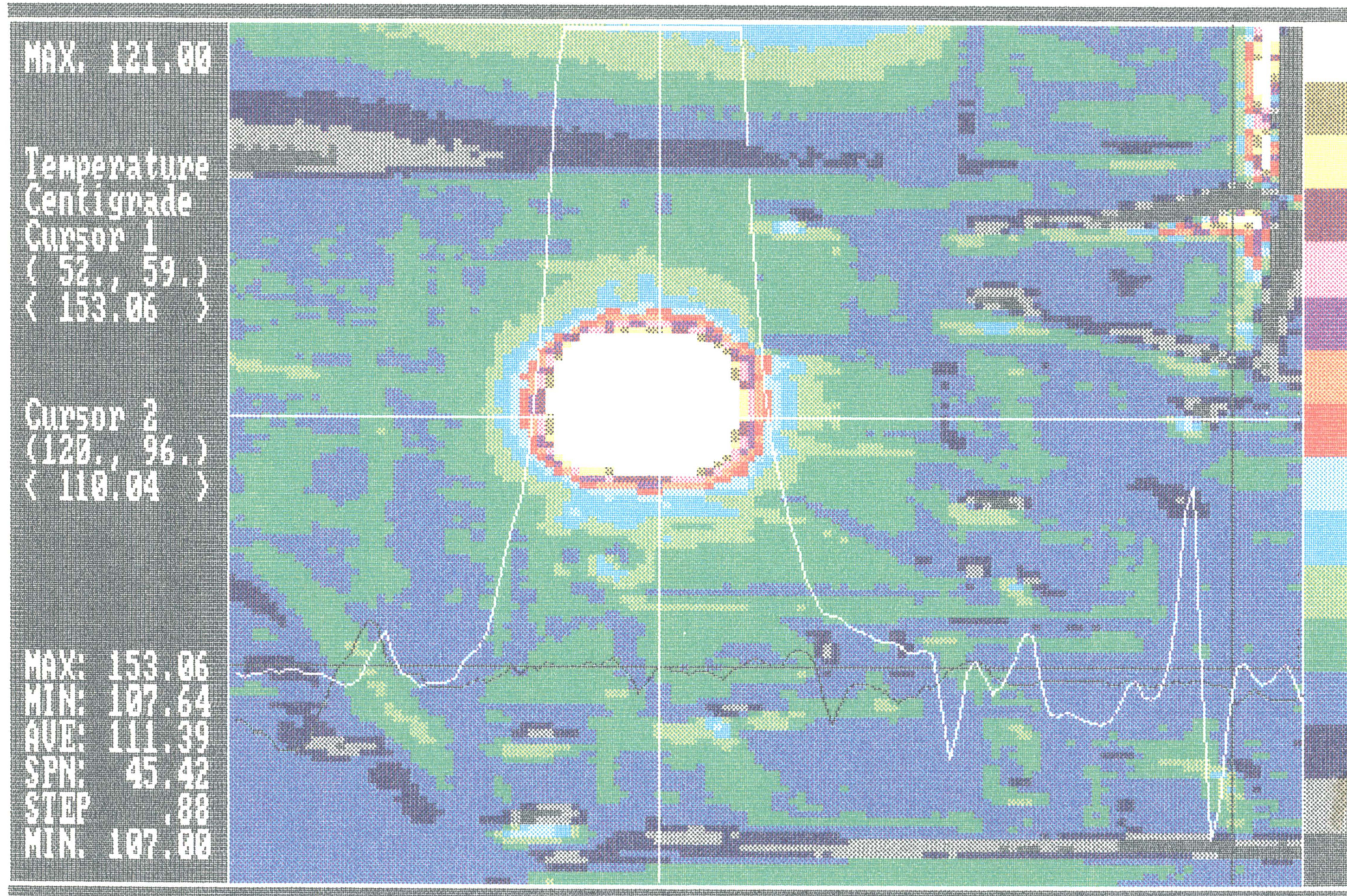

Figure 13. Temperature contours of a powered filter circuit mounted on a 110 C stage

paramount importance. These hot spots must be identified and measured. Ultimately, these high temperatures must be reduced so that one overheated device does not fail and thereby cause the entire hybrid to fail. In the study of hybrid operating temperatures, the variations in temperatures throughout the assembly are normally not critical, provided that each individual device does not exceed its own temperature limit. However, extreme temperature gradients need to be avoided in order to eliminate thermal stresses that could result in fatigue failure.

Chapter 6

Conclusions and Recommendations

The IR thermal imager has proven to be an accurate instrument for the measurement of the surface temperatures on hybrid circuits. The accuracy is excellent, within 1°C, at high temperatures for high emissivity materials. Six areas for improvement of the measurement technique have been determined. Most of these proposed improvements are methods of calibrating the temperature measurement or of verifying the temperature prediction of the software. Two of the proposed improvements would make obtaining temperature measurements more convenient for the operator. A suggestion for improving the software model is also made. The final recommendation specifies guidelines for designing the next test circuit.

The accuracy of the imager temperature calculation could be further specified in one of three ways. The first would be to measure the temperature distribution over the 5 cm x 5 cm heater stage area. A 5x5 matrix of 36-gauge type J thermocouples could be mounted to the stage with thermal grease or conductive epoxy. The heater temperature could then be increased in five steps of 20°C and allowed to reach

thermal equilibrium at each step. This data would provide a temperature map of the stage and would indicate any significant variations from uniform temperatures. The test could be repeated with a layer of insulation above the stage to show the reduction of temperature due to natural convection from the stage.

The second calibration technique would involve mounting a small thermocouple or thermistor to the resistor surface of the test circuit using thermally conductive epoxy. This would allow a comparison of the imager temperature measurement to the thermocouple or thermistor measurement. The third technique would be a comparison of the imager measurements to the results from the application of thermal paint to the surface of the resistor in the test circuit.

Two additional improvements are imperative to maximizing the usefulness of the temperature data obtained from the imager. The anomalous variations in the radiance and emissivity data in the "edge-effect region" must be understood or eliminated. In addition, the calculation of emissivities greater than 1.0 must be interpreted.

The experiments performed for this comparison of predicted and measured temperatures had limited radiation and convection heat transfer. The ability to mathematically model the heat transfer of operating hybrid circuit requires the verification of the software for various combinations of radiation, convection, and conduction heat transfer that occur in hybrids. A series of measurements could be made on the test circuit after it has been insulated with Plexiglas. The Plexiglas would be placed between the hybrid substrate and the heater stage. The increased thermal conduction resistance would necessitate the use of emissivity values from previous calculations in order to obtain the temperatures from radiance data, because the emissivity correction procedure will not work with insulators. A series

of temperature increases due to several increases in the conduction thermal resistance could then be compared to temperatures predicted by the software model.

The measurement of the stage temperature,T_o, can be improved by mounting a thermocouple in a hole drilled in the imager stage. More recent models of Barnes thermal imagers include this feature. The thermocouple would provide more accurate measurements of the stage temperature and would simplify the measurement procedure.

The process of positioning the test circuit vertically requires substantial operator patience in addition to a fixture that holds the heater stage. A plywood stand was cobbled for Phase III and IV tests. A metal stand, with x,y,z positioning capabilities, would make this process much easier. The x,y,z positioning accuracy does not need to be precise; $\pm$1.5 mm would be sufficient since final focusing is done with the 3X lens adjustment after the mirror angle, x,y and θ stage positioning and zoom are set.

The lumped-parameter one-dimensional thermal model could be improved in future software. The 6°C difference between the measured and predicted temperature, described in Section 5.1.5, might be reduced if a conduction spread angle is considered. The spread angle would allow the conduction heat transfer resistance to be varied without changing the convection and radiation heat transfer area. A more sophisticated, yet still simple, two-dimensional model could be developed using a network of thermal resistances and solved with SPICE.

Future temperature measurements will be obtained from hybrid circuits that are more complex than one resistor. Care must be used in the design of such circuits. One possibility for the next test circuit would be to increase the number of thick-film resistors to two or three. The resistances should be chosen to give a 5 – 10°C temperature rise for an applied voltage 40V, the maximum voltage readily

available in the lab. A symmetric circuit layout would simplify the computer analyses and reduce computation time.

Bibliography

Andrews, James A., Mahalingham, L. M., and Berg, Howard M., 1981, "Thermal Characteristics of 16- and 40-Pin Plastic DIPs," *IEEE Trans. on Components, Hybrids and Manufacturing Technology,* Vol. CHMT-4, No. 4, pp.455-461.

Antonetti, Vincent W., and Simmons, Robert E., 1985, "Bibliography of Heat Transfer in Electronic Equipment," *IEEE Transactions on CHMT,* Vol. CHMT-8, No. 2, pp.289-295.

Arnold, James T., 1982, "Thermal Analysis To Determine Integrated Circuit Chip Hot Spot Temperatures," *IEPS Proceedings,* pp.65-76.

Atkinson, K., 1985, *Elementary Numerical Analysis,* NY: John Wiley and Sons

Bar-Cohen, A., Kraus, Allan D., and Davidson, Steven F., 1983, "Thermal Frontiers in the Design and Packaging of Microelectronic Equipment," *Mechanical Engineering,* Vol. 105, No. 6, pp.53-59.

Barnes Instruction Manual, Infrared Micro Imager, Model RM-50 #TM-RM50-278 EDO Corporation, Barnes Engineering Division, Shelton, Connecticut

Baxter, Gene K., 1977, "A Recommendation of Thermal Measurement Techniques for IC Chips and Packages," *Proc. Int'l. Reliability Physics Symp, Las Vegas, NV,* Apr 12-14, 1977, pp.204-211.

Beccue, Phil., 1987, "Micro-Based Thermal Model for Power Hybrids," *Power Conversion and Intelligent Motion,* February 1987, pp.12-18.

Berman, Herbert L., 1983, "Infrared Temperature Measurement," *Test and Measurement World,* October 1983, pp.88-101.

Buchanan, R. C., and Reeber, M. D., 1973, "Thermal Considerations in the Design of Hybrid Microelectronic Packages," *Solid State Technology,* February 1973, pp.39-43.

Chu, Richard C., 1986, "Heat Transfer in Electronic Systems," *Proceedings of the Eighth International Heat Transfer Conference*, Ten, C. L., et al., ed. Hemisphere Publishing Corporation, Washington, D.C., Vol. 1 pp.293-305.

Conway, T. G., 1987, "Using Thermal Images to Measure Temperature," *Mechanical Engineering,* Vol. 109, No. 6, pp.32-34.

David, Richard F., 1977, "Computerized Thermal Analysis of Hybrid Circuits," *IEEE Trans. on PHP,* Vol. PHP-13, No. 3, pp.283-290.

David, Richard F., 1981, "Correction to Computerized Thermal Analysis of Hybrid Circuits," *IEEE Trans. on CHMT,* Vol. CHMT-4, No. 2, p.230.

Dettmer, E. S., & Charles, H. K., Jr., 1987, Fundamental Characterization of Aluminum Nitride and Silicon Carbide for Hybrid Substrate Applications. *Int'l J. for Hybrid Microelectronics,* Vol. 10, No. 2, pp. 9-18.

Donahoe, Daniel N., 1986, The Bedrock of Electronics Packaging. *Mechanical Engineering,* Vol. 108, No.10, pp.62-63.

Doshay, I., 1984, Reliability Impact of Thermal Design. *IEPS Proceedings,* 1984, pp.307-317.

Eid, Jeffrey C., 1986, Spreadsheets for Thermal Analysis. *Machine Design,* Oct 23,1986, Vol. 58, No. 25, pp.121-125.

Ellison, Gordon N., 1984, *Thermal Computations for Electronic Equipment.* New York: Van Nostrand, Rienhold Co, 1984.

Elmer-DeWitt, Phillip., 1985, A Sleek, Superpowered Machine. *Time,* June 17,1985, p.53.

Engel, Peter A., and Lim, Chun K., 1986, Finding the Stresses with Finite Elements. *Mechanical Engineering,* Vol.108, No.6, pp.46-50.

Engelhardt, Robert E., and Hewgley, W. W., 1973, *Thermal and Infrared Testing. Nondestructive Testing, A Survey, NASA-SP-5113.* NASA, 1973, Chapter 6, pp.119-140.

Fitzsimons, James., 1987, Private Communication. EDO Corporation, Barnes Engineering Division, Shelton, Connecticut, October, 1987.

Frank, L. E., and Halpern, A. R., 1983, Computer-Aided Generation of Detailed Thermal Models. *IEPS Proceedings,* 1983, pp.226-241.

Gold, Robert D., 1977, Materials Selection in Hybrid Product Design. *Solid State Technology,* January 1977, pp.31-35.

Griffin, D. D., 1968, Infrared Microradiometry- Precision and Accuracy Considerations Applicable to Microcircuit Temperature Measurements. *Materials Evaluation,* October 1968, pp.215-220.

Holman, J. P., 1976, *Heat Transfer, 4th Ed.*. New York: McGraw-Hill, 1976.

Hopkins, D. C., Jovanovic, M. M., Lee, F. C., and Stephenson, F. W., 1987, Two-Megahertz Off-Line Hybridized Quasi-Resonant Converter. *Proc. Second Annual IEEE Applied Power Electronics Conference and Exposition- APEC,* March 2-6, 1987, pp.105-114.

Jardine, Linda., 1985, Hybrid Industry Forecast. *Nepcon West Proceedings,* 1985, p.331.

Johnson, Eric A., and Seraphim, Donald P., 1986, Fabricating Advanced Circuit Boards. *Mechanical Engineering,* Vol. 108, No.10, pp.58-61.

Kallis, James M., Samuels, Albert H., and Stout, Roger P., 1984, True Temperature Measurements of Electronic Components Using Infrared Thermography. *IEPS Proceedings,* 1984, pp.616-627.

Kaye, Harvey., 1985, Junction-Temperature Planning Boosts Product Reliability. *EDN,* April 18,1985, pp.225-235.

Kays, W. M., and Crawford, M. E., 1980, *Convective Heat and Mass Transfer 2nd Ed.*. New York: McGraw-Hill, 1980.

Khol, Ronald (Ed.)., 1986, CAD/CAM Reference Issue, *Machine Design* Vol. 58, No. 14, pp.64-76.

Kline, S. J., & McClintock, F. A., 1953 Describing Uncertainties in Single-Sample Experiments. *Mechanical Engineering,* Jan 1953, pp. 3-8.

Kraus, Allan D., and Bar-Cohen, Avaram., 1983, *Thermal Analysis and Control of Electronic Equipment.* Washington: Hemisphere Pub. Corp., 1983.

Kraus, Allan D., Chu, Richard C., and Bar-Cohen, Avram., 1982, Thermal Management of Microelectronics: Past, Present and Future. *Computers in Mechanical Engineering,* October 1982, pp.69-79.

Landis, Richard C., 1986, The Next Wave: Mounting on the Surface. *Mechanical Engineering,* Vol. 108, No. 10, pp.64-68.

Lynch, Charles T., ed., 1975, *CRC Handbook of Material Science. Nonmetallic Materials and Applications* Cleveland, Ohio: CRC Press, Vol. III, p.5.

Madding, Robert P., 1983, Science behind thermography. *Thermal Infrared Sensing Diagnostics (Thermosense V,* 1983, Vol. 371, pp.2-9.

Markstein, Howard W., 1984, Airborne Radar Jammer is Packaged for Density and Reliability. *Electronic Packaging and Production,* October 1984, pp.42-48.

Marriott, Douglas F., 1986, Letter to the editor. *Mechanical Engineering*, Vol. 108, No. 12, p.2.

Metal Progress,, 1987, The Coming Revolution in Electronic Packaging. January 1987 Vol. 131, No. 1, pp.84-92.

Mizuno, K., 1983, Packaging Trade-offs Between Large Area Hybrids and Small Area Hybrids. *IEPS Proceedings*, 1983, pp.464-475.

Modern Plastics Encyclopedia, 1985-86, New York: McGraw-Hill, Vol. 62, No. 10A

Moffat, Robert J., 1987, Experimental Methods for Air Cooling of Electronic Components. *International Symposium of Cooling Technology for Electronic Equipment, Honolulu, Hawaii, Keynote Lecture*, March 1987, pp.1-31.

Munis, Richard H., and Kaplan, Herbert., 1983, What's out there: state-of-the-art survey of thermal infrared instrumentation. *Thermal Infrared Sensing Diagnostics (Thermosense V*, 1983, Vol. 371, pp.10-17.

Murtuza, Masood., 1982, Computer-Generated models Abridge Thermal Analysis of Packaged VLSI. *Electronics*, Feb 10, 1982, pp. 145-148.

Oettinger, Frank F., 1984 Thermal Evaluation Of VLSI Packages Using test chips- A Critical Review. *Solid State Technology*, February 1984, pp.169-179.

Oktay, Sevgin, Hannemann, Robert, and Bar-Cohen, Avram., 1986, High Heat from a Small Package. *Mechanical Engineering*, Vol. 108, No. 3, pp.36-42.

Ozisik, M. Necati., 1980, *Heat Conduction*. NY: John Wiley and Sons

Parks, Paul F. Sr., 1987, President's Corner. *Inside ISHM*, ISHM, Reston, VA July-August 1987, p.4.

Pearson, Keith V., 1986, Printed Circuit Board Fault Detection and Isolation Using Thermal Imaging Techniques. *Thermal Imaging*, 1986, *636*, pp.122-125.

Peterman, David, and Workman, Wilton., 1967, Infra-Red Radiometry of Semiconductor Devices. *Microelectronics and Reliability*, 1967, Vol. 6, pp.307-315.

Pitzele, Lennart D., 1986, *The System Fabrication of a 10 MHz, DC-DC Switching Power Supply. MIT.* Master's thesis, September 1986.

Pletcher, Richard H., and Patankar, Suhas V., 1983, Computers in Analysis and Design. *Mechanical Engineering*, Vol. 105, No. 6, pp.73-79.

Pound, Ronald., 1984, Thermal CAD brings Hot Spots Under Control. *Electronic Packaging and Production*, April 1984, pp.56-61.

Reddy, J. N., 1984, *An Introduction to the Finite Element Method.* New York: McGraw-Hill Book Company, 1984.

Rodriquez-Corre, Manuel., 1984, Finite-Difference Analysis Simplifies Heat Transfer Problems. *Machine Design,* December 6, 1984, pp.128-132.

Rohsenow, W. M., and Harnett, James P., (Eds.), 1973, *Handbook of Heat Transfer.* New York: McGraw-Hill, 1973, pp.19-47.

Rucker, Paul D., 1987, Private Communication. ITT Corporation, Roanoke, Virginia September, 1987.

Schorry, Robert E., 1987, Better, Not Dumber. *Mechanical Engineering.* Vol. 109, No.2, p.2.

Scott, Donald E., 1987 *An Introduction to Circuit Analysis, A Systems Approach.* New York, NY: McGraw-Hill, 1987

Seely, J. H., and Chu, R. C., 1972, *Heat Transfer in Microelectronics Equipment.* New York, NY: Marcel Decker, 1972.

Semiconductor International,, 1987, Aluminum Nitride. June 1987, p.42.

Sharpless, Edward N., 1984, Using Liquid Crystals For Component, PCB Thermal Evaluations. *Electri.onics,* December 1984, pp.41-44.

Shepherd, Jay W., 1987a, A discussion of emissivity correction and its application in infrared microimaging. *Proc. of SPIE- The International Society for Optical Engineering,* May 18-20, 1987, *780,* pp.130-138.

Shepherd, Jay W., 1987b, Private Communications. EDO Corporation, Barnes Engineering Division, Shelton, Connecticut, November, 1987.

Siegel, Robert, and Howell, John R., 1981, *Thermal Radiation Heat Transfer.* Washington: Hemisphere Publishing

Sonnad, Vijay., 1983, The Finite Element Method in Convective Heat Transfer. *IEPS Conference Proceedings Supplement,* pp.s21-s22.

Steel, Jeffrey M., 1985, Selecting an Analysis Program. *Computer Aided Engineering,* September 1985, pp.72-73.

Steinberg, David S., 1980, *Cooling Techniques for Electronic Equipment. Newman.* New York: John Wiley and Sons, 1980.

Szekely, George S., 1987, ISHM Glossary of Hybrid-Circuit Terms. Summer 1987. ISHM, Reston, VA

Thermalloy Inc., 1983, Catalog # 84-HS-3 Semiconductor Accessories. P. O. Box 810839, Dallas, TX 75381-0839: 1983.

Thompson, Edward C., 1985, Design Criteria For Thick and Thin Film Hybrid Circuits. *NEPCON West,* 1985, pp.351-370.

Vanzetti, Ricardo., 1972 *Practical Applications of Infrared Techniques*. New York: John Wiley and Sons, 1972

Walton, Anthony J., Marsden, Barry J., and Scurr, David., 1981, The Application of the Finite Element Technique to the Design and Analysis of Hybrid Microelectronic Circuits. *ISHM Int'l. Symposium*, 1981, pp.370-375.

Weast, Robert C., (Ed.)., 1979, *CRC Handbook of Chemistry and Physics, 60th Ed.*. Boca Raton, Florida: CRC Press Inc., 1979.

Zimmer, Carl R., 1983, Computer Simulation of Hybrid Integrated Circuits Including Combined Electrical and Thermal Effects. *ELECTROCOMPONENT Science and Technology*, 1983, *10*, pp.171-176.

Appendix A

Operation Procedures and Equipment

A.1 Tools required for set-up of Barnes Imager

The set up of the RM-50 Barnes imager required 2 people to uncrate the instruments and took one-half day to set up.

The tools necessary for this set-up included:

Small flat screwdriver to attach cables
Liquid nitrogen, dewar, eye goggles,funnel
Wire ties to organize power cords
8 in. wire cutters to cut wire ties used in shipment
Containers for lense storage
8 inch long cotton swabs

A.2 Materials required for 30 hours of Imager operation

Item	Quantity
5.25 inch DSDD diskettes with labels	12
Liquid nitrogen	4 liters
Thermal grease	< 1 fluid oz.
Solvent for thermal grease	< 1 fluid oz.
Swabs, 8 inches long	16
Wire ties to secure wires in experiment	10

A.3 Expendable Supplies replaced at intervals > 30 hours

Item	Quantity
Masking tape to secure wires in experiment	1 roll
Duct tape to secure towel in experiment	1 roll
Ink jet cartridge, color	--
Ink jet cartridge, black	--
Paper for printer	--
Towel, coarse	1

Appendix B
SPICE Operation Instructions

To run spice a file with filetype 'spice' must be created,

eg., filename spice a

The following is an example from Scott (1987) page 705.

Some simplifications have been made for clarity.

```
**********************************************************************
CIRCUIT EXAMPLE IN DONALD E. SCOTT'S BOOK
V1 1 0 1
I2 3 2 2
R1 1 2 2
R2 2 0 3
R3 3 0 2
R4 1 3 8
* NOTE .SENS AND .TF REMOVED FOR CLARITY
.END
**********************************************************************
```

The first line in this example is a title that is not processed but is printed at the beginning of the output. Lines that begin with V and I are voltage and current sources, respectively. This voltage source, V1, is connected from node 1 to node 0 and has an output of 1 volt. Resistors are input in the same way, for example R3 is connected between nodes 3 and 0 and has a value of 2 ohms. Any line in the spice file that has a '*' in the first column is a comment line that is not used in the calculation. The spice analysis ends where the '.end' line is included.

After this file is created it can be run on VM2 using these commands:

LDISK EELIB

SPICE 'filename'

The output will be sent to your readerlist with the name 'SPICE OUTPUT'

Appendix C

Supplementary Imager Operation Instructions

1) Perform the emissivity correction procedure at least every few hours to be sure that it is correct.

2) Run the imager with the fan off to reduce vibrations of the heater stage. The detector will remain cool enough for efficient operation without the fan.

3) There is no warning light on the RM-50 to indicate a low liquid nitrogen level. The dewar requires refilling approximately every 4 hours. Damage will not occur if the imager runs out of liquid nitrogen, but the sensitivity of the detector will be impaired.

4) To prevent icing refill the dewar before the liquid nitrogen level goes below 1″ in depth in dewar.

5) Liquid nitrogen can be added to the dewar without powering down the imager.

6) If liquid nitrogen spills over the dewar during refilling then the imager must be allowed 2 hours to restabilize before resuming measurements.

7) The imager should be allowed a 30 minutes warm-up period before the first measurements are taken. This allows thermal expansion of the optics and mirrors to occur, and it reduces the Narcissus effect.

8) The imager detector has a higher sensitivity at higher temperatures ($>70°C$) because there is more energy radiated in the detected wavelength range.

9) Apply thermal grease to the thermocouples used to measure stage temperature.

10) Mechanically support the stage with shims to prevent x, y, and θ motion after the IR lens has been focused. Motion can be caused by from backlash in the threads of the micrometers, the vertical adjustment, or the θ adjustments.

11) To change the size of the color printout, use this key sequence in the CompuTherm software:

Shift-PrtSc

H

16

Carriage Return

Shift-PrtSc

W

22

Carriage Return

Shift-PrtSc

P

N

Carriage Return

This will print the output in the 16x20 size chosen; other sizes are available. A 16x20 plot is 10.16 cm x 12.7 cm (4 in x 5 in) because the 16 & 20 are both multiplied by 6.35 mm (0.25 in) to get the outside dimensions of the plot.

Appendix D

Software not chosen

The following software packages were evaluated against the criteria given in Chapter 4 and rejected. They are included here for reference purposes.

Name: ADINAT
Description: Commercially available FEM code for conduction
Source: Abuaf and Kadambi, 1985
Why it was not used: An involved FEM code was more complicated than we wanted to get.

Name: CINDA (Chrysler Improved Numerical Differencing Analyzer
Description: This is on of the most popular finite difference codes available.
Source: COSMIC, NASA's Computer Software Management and Information Center. Frank and Halpern, 1983
Why it was not used: The cost of leasing this from COSMIC seemed too expensive and the start-up time for a new user was deemed prohibitive.

Name: EMP
Description: Steady State Thermal Analysis of 300 unknown temperature points.
Source: EMP Engineering
P. O. Box 1000
Nesconset, NY 11767
(516) 361-8921
Why it was not used: $875 purchase price.

Name: FERO
Description: This finite difference package is used at Motorola in the analysis of DIPs.
Source: Andrews et al., 1981
Why it was not used: This is company proprietary.

Name: IGSPICE
Description: This is an improved version of SPICE that includes graphics which are useful for transient analyses.
Source: This is available in the VPEC VAX at VPI&SU.
Why it was not used: The graphic capabilities were not required.

Name: I/TAS (Interactive Thermal Analysis System)
Description: Finite Difference solutions for steady state and transient problems.
Source: R. Warriner Associates
3838 Carson Street, Suite 300
Torrance, CA 90503
Why it was not used: Cost was $450 for 350 nodes and 600 connectors

Name: PCAP (Princeton Circuit Analysis Program)
Description: This is similar to SPICE.
Source: This is available on the VPI&SU mainframe.
Why it was not used: Less documentation was available for this than for SPICE so this was not pursued.

Name: PCSPICE/PSPICE
Description: SPICE for a PC
Source: Microsim Corp.
1401 Yorba Street, Suite 202
Tustin, CA 92680
(714)731-8091
Notes: Some VA Tech faculty members have copies of this.
Why it was not used: The mainframe terminals are easier to get access to and SPICE will do the same job.

Name: RAVFAC
Description: NASA developed this for analysis of high temperature processing of semiconductors.
Source: Pound, 1984
Why it was not used: This did not seem useful so it was not pursued.

Name: SINDA
Description: see CINDA

Name: TASS
Description: A steady state thermal analysis specifically written for electronic circuits. A transient analysis is available.
Source: Intercept Software
3425 South Bascom Avenue
Campbell, CA 95008
(408) 377-4998
Notes: It will accept 300 nodes
Why it was not used: The $395 purchase price.

Name: TAMS (Thermal Analyzer for Multilayer Systems)
Source: Ellison, 1984
Notes: Restricted to 3-D slabs, other geometries may be represented by a thermal network (page 218).
Why it was not used: This is written in FORTRAN IV and was not readily compatible with the IBM mainframe compilers available. The Vax compiler may be useful; this was never tried.

Name: TASIC
Description: Uses Green's function to evaluate heat source temperatures for sources on a homogeneous substrate only. This is similar to TAMS.
Source: Fritsch, 1983
Why it was not used: This was not followed up because it only studied substrates rather than an assembly of components to a substrate.

Name: TDS (Thermal Design System)
Description: Thermal modeler
Source: Sampson Technical Consultants, Inc.
P.O. Box 4828
Auburn, CA 95604
(916) 823-3859
Notes: Written in FORTRAN. It gives and automatic calculation of convective heat transfer coefficients.
Why it was not used: The $6500 price.

Name: THTD (Transient Heat Transfer Version D)
Description: It is reliable because it was written in 1958 using finite differences.
Notes: (Baxter and Anslow, 1977)
Why it was not used: The nodal network solved by the finite difference method is not well suited for the analysis of circuit assemblies.

Name: TNETFA (Transient Network Thermal Analyzer)
Description: Steady state and transient analysis and velocity potential solutions.
Source: Ellison, 1984
Notes: Approximately 1700 lines of FORTRAN IV that allow 650 nodes and 4000 connectors. There is a 50 node limit to multiple surface radiation exchange. This seemed well suited for the analysis of circuit assemblies. This may be purchased from:

Thermal Computations, Inc.
3876 S. E. Bliss Court
Hillsboro, Oregon 97123

Why it was not used: The compiler problems encountered with TAMS and the effort required to type in 1700 lines of code.

Name: TXYZ
Description: FORTRAN for transient analysis of 3-D slabs.
Source: NBS
Notes: Available at no charge (Oettinger, 1984)
Why it was not used: Wanted to study assemblies not slabs.

Appendix E

Specifications

E.1 Barnes RM-50 Specifications

Table 1. PERFORMANCE SPECIFICATIONS

Field of View	See Table 2
Lines Per Frame	64 or 128 (selectable)
Elements Per Line	42
Frame Time	1 Second, 2 Second (selectable)
Spatial Resolution	See Objective Table
Temperature Sensitivity	0.1°C for a 30°C Target
Temperature Measuring Range	Ambient to 200°C*
Working Distance	See Objective Table
Detector	Liquid Nitrogen-Cooled InSb** — 4 Hour Hold Time
Electrical	
Input Power	115/ 230V, 50-400 Hz 100 Watts
Mechanical	
Size	23" H x 20" W x 16" D (58.4 x 50.8 x 40.6 cm)
Weight	90 Lbs. (40.8 kg.)

* Range extender available for measuring to 600°C.
** Adaptable to other cooled detectors as required by the application.

Table 2. TYPICAL INTERCHANGEABLE OBJECTIVES

Typical Interchangeable Objectives

Power***	Working Distance	F.O.V. (Square)
100X	0.3"(0.76 cm)	0.025"(0.635 mm)
40X	1.0"(2.54 cm)	0.064"(1.626 mm)
10X	4.0"(10.16 cm)	0.25" (6.350 mm)
Variable 3X or Less	30" (76.20 cm) / ∞	1.0" (25.400 mm) / 2.5°

Power***	Spatial Resolution††
100X	0.0006"(0.015 mm)
40X	0.0015"(0.038 mm)
10X	0.006" (0.15 mm)
Variable 3X or Less	0.030" (0.76 mm) (1.0 mr)

Note: Electronic zoom multiplies all powers up to 3 times.

*** The listed power indicates the number of times the image on the viewing screen is larger than the object on the instrument stage.
†† Half power points. For single point transient measurements total spot size is approximately 1.5 x this value.

Figure 14. Barnes RM-50 thermal infrared imager specifications (Barnes Manual)

Appendix F

UNCER FORTRAN Listing

```
C
C   VERSION 1.7 12-3-87
C
C   THIS PROGRAM WAS WRITTEN TO MAKE A COMPARISON BETWEEN THE EFFECT
C   OF RADIATION, CONVECTION AND CONDUCTION
C   RESISTANCE PREDICTIONS IN A SIMPLE RESISTOR MODEL
C
C   VARIABLE DECLARATIONS
C
    REAL R,V,I,TA,TW,WTA,WTO,WTW,RR,RV,RD,WPE,
   $     WPEDVP,POWER,DTJ,DTA,DTW,DTO,DRR,DRV,DRD,WTJ(20,10,6),
   $     WRD,WRR,WRV,TJ,C1,WI,WV,WR,WIDIVI,
   $     WTJRAT(20,10,6),WRDRAT(20,10),WRVRAT(20,10)
C
    INTEGER A,B,C
C
C
C    A,B,C    LOOP COUNTERS
C    COUNT  ITERATION COUNTER
C    R      MEASURED RESISTANCE VALUE    UNITS: OHMS
C    V      MEASURED VOLTAGE VALUE       UNITS: VOLTS
C    I      MEASURED CURRENT VALUE       UNITS: AMPS
C    WI,WR,WV     VARIATION IN CURRENT ,RESISTANCE ,VOLTAGE
C                 MEASUREMENTS    UNITS: SAME AS VARIABLE
C
C              UNITS FOR ALL TEMPERATURES: DEGREE KELVIN
C              UNITS FOR ALL THICKS: CM   FOR CONVENIENCE
C
C    TA,TO,TW    TEMP IN AMBIENT AIR, IN SINK, AT WALL
C    TJ    TEMP IN RESISTOR "JUNCTION"
C    EPS     EMISSIVITY
C    WTA,WTO,WTW   VARIATION IN TEMP IN AMBIENT AIR, IN SINK, AT WALL
C    WRR,WRV,WRD   VARIATION IN THERMAL RESISTANCE FOR
C                  RADIATION,CONVECTION,CONDUCT
```

```
C    WRVRAT(B,C)  RATIO OF  VARIATION IN THERMAL RESISTANCE FOR
C                 CONVECTION
C    WRDRAT(A,C)  RATIO OF VARIATION IN THERMAL RESISTANCE FOR
C                 CONDUCTION
C    RR,RV,RD     THERMAL RESISTANCE FOR RADIATION,CONVECTION,CONDUCT.
C                      UNITS: WATTS
C    POWER    POWER CALCULATED WITHOUT ERROR
C                      UNITS: WATTS
C    DTJ,DTO,DTW,DTA  THE PARTIAL DERIVATIVE OF POWER CALCULATED
C                  FROM THERMAL VARIABLES WITH RESPECT TO TJ,
C                  TO,TW,TA
C    DRV,DRR,DRD  THE PARTIAL DERIVATIVE OF POWER CALCULATED
C               FROM THERMAL VARIABLES WITH RESPECT TO
C               RV,RR,RD
C    WTJ(A,B,C)     VARIATION IN CALCULATED TJUNCTION
C    WTJRAT(A,B,C)  RATIO OF VARIATION IN CALCULATED TJUNCTION
C                 WTJRAT  = WTJ/TJ
C    COND    THERMAL CONDUCTIVITY W/SQ CM DEG C
C    AREA(10,10)    HEAT TRANSFER AREA(10,10) SQ CM
C    THICK   THICKNESS OF SUBSTRATE   CM
C
C
     COMMON THICK,SIGMA,POWER,TA,TW,COND,A,B,C,
    $      AREA(20,10),EPS(6),H(20,10),TO(20)
     EXTERNAL DELTA
     EXTERNAL DDELTA
C            FUNCTIONS USED IN NEWTON SUBROUTINE
C
C     BEGIN PROGRAM
C
     TOL=0.00001D0
C       TOLERANCE FOR ITERATION
     WTJTMP=0.33D0
C             DEG K
     WTOP=0.0D0
C             DEG K
     SIGMA=5.669E-12
C         UNITS W/SQ CM DEG K**4
C
     READ(8,*) R,V,WR,WV,TA,TO(1),
    $ TW,WTA,WTO,WTW,EPS(1),H(1,1),COND,THICK,
    $ AREA(1,1),
    $ WEPS,WH,WCOND,WTHICK,WAREA
C
C      PRELIMINARY CALCULATIONS
C
     I=V/R
     POWER=V*I
C
C     ECHO INPUT DATA AND PRELIMINARY CALCULATIONS TO FILE
C
C      CALCULATE THE UNCERTAINTY RATIOS
C
      RRES=WR/R
      RVOLT=WV/V
      RTA=WTA/TA
      RTO=WTO/TO(1)
      RTW=WTW/TW
      RAREA=WAREA/AREA(1,1)
      RCOND=WCOND/COND
      RTHK=WTHICK/THICK
      RH=WH/H(1,1)
```

```
      REPS=WEPS/EPS(1)
C
 222  WRITE(9,225) R,WR,RRES,V,WV,RVOLT,TA,WTA,RTA,TO(1),WTO,RTO,TW,WTW,
     $ RTW,AREA(1,1),WAREA,RAREA,COND,WCOND,RCOND,
     $ THICK,WTHICK,RTHK,H(1,1),WH,RH,EPS(1),WEPS,REPS
 225  FORMAT('  UNCERTAINTY INPUT DATA' ,// ,
     $ ' VARIABLE        UNIT    VALUE      UNCERTAINTY     RATIO',/,
     $ '=======================================================',
     $ '============================',/,
     $ 'RESISTANCE,      OHMS   ',3(F10.5,2X),/,
     $ 'VOLTAGE,         VOLTS  ',3(F10.5,2X),/,
     $ 'AMBIENT, TA      DEG K  ',3(F10.5,2X),/,
     $ 'HEATER STAGE, TO  DEG K  ',3(F10.5,2X),/,
     $ 'WALL TEMP TW      DEG K  ',3(F10.5,2X),/,
     $ 'H.T. AREA        SQ CM  ',3(F10.5,2X),/,
     $ 'THERMAL COND      W/CM K ',3(F10.5,2X),/,
     $ 'HYBRID THICKNESS  CM     ',3(F10.5,2X),/,
     $ 'CONV. HT COEF. W/SQ CM K ',3(F10.5,2X),/,
     $ 'EMISSIVITY        --     ',3(F10.5,2X),///)
      WRITE(9,220)TOL,WTJTMP
 220  FORMAT( 'ITERATION TOLERANCE       ', (F10.5,2X),/,
     $ 'BASED ON WTJTMP = ',F7.2,//,
     $ ' ',///)
C
      WRITE(10,3100)
 3100 FORMAT('//A014SWM JOB 543D5,STEVEMAC,TIME=1,REGION=1056K   ',/,
     2 '/*PRIORITY STANDARD                              ',/,
     3 '/*ROUTE PRINT VTVM2.STEVEMAC                           ',/,
     4 '/*JOBPARM LINES=1,ACCTPG                            ',/,
     5 '//STEP1 EXEC SAS                              ',/,
     6 '//SYSIN DD *                              ',/,
     7 'GOPTIONS DEVICE=VER80 NOTEXT82 NOCHARACTERS NOSYMBOL; ')
C
C   OUTSIDE LOOP  -- USED IN PREVIOUS ANALYSES
C
      DO 6000  C=1,1
C
      IF(C.GT.1)THEN
          EPS(C)=EPS(C-1)+WEPS/5.0D0
      END IF
      IF (C.EQ.1) THEN
      WRITE(10,3200)
 3200 FORMAT('DATA ONE; ',/,'INPUT A   B   C WTO  ',
     $   ' DIFP    WTJ;  ',/,'CARDS; ')
      END IF
      IF (C.EQ.2)THEN
      WRITE(10,3205)
 3205 FORMAT('DATA TWO; ',/,'INPUT A   B   C WTO  ',
     $   '   DIFP    WTJ;  ',/,'CARDS; ')
      END IF
      IF (C.EQ.3) THEN
      WRITE(10,3215)
 3215 FORMAT('DATA THREE; ',/,'INPUT A   B   C WTO  ',
     $   ' DIFP    WTJ;  ',/,'CARDS; ')
      END IF
      IF (C.EQ.4)THEN
      WRITE(10,3225)
 3225 FORMAT('DATA FOUR; ',/,'INPUT A   B   C WTO  ',
     $   ' DIFP   WTJ;  ',/,'CARDS; ')
      END IF
      IF (C.EQ.5)THEN
      WRITE(10,3229)
 3229 FORMAT('DATA FIVE; ',/,'INPUT A   B   C WTO  ',
```

```
   $  ' DIFP   WTJ;  ',/,'CARDS; ')
    END IF
    IF (C.EQ.6) THEN
    WRITE(10,3236)
3236 FORMAT('DATA SIX; ',/,'INPUT A   B   C WTO  ',
   $  ' DIFP   WTJ;  ',/,'CARDS; ')
    END IF
C
         DO 2000 B=1,1
              DO 1000 A=1,20
    IF(B.GT.1) THEN
C         AREA(A,B)=AREA(A,B-1)
C         H(A,B)=H(A,B-1)
    END IF
    IF((A.GT.1).AND.(B.EQ.1))THEN
        AREA(A,B)=AREA(A-1,B)
        TO(A)=TO(A-1)+WTO/19.0D0
C         AREA(A,B)=AREA(A-1,B)+WAREA/19.0D0
C         H(A,B)=H(A-1,B)+WH/9.0D0
C             INCREMENT THESE LATER
    END IF
C
    H(A,B)=H(1,1)
C                DO NOT INCREMENT H THIS TIME
    TJINIT=TO(1)
C
    ITMAX = 10
C        MAX NO ITERATIONS
    CALL NEWTON(DELTA,DDELTA,TJINIT,TOL,ITMAX,TJ,IER)
C       DELTA   FUNCTION USED
C       DDELTA  DERIVVATIVE OF FUNCTION USED
C       TJINIT INITIAL GUESS OF TJ
C       TOL    TOLERANCE FOR ERROR IN ROOT FINDING
C       ITMAX  MAX NUMBER OF ITERATIONS
C       OUTPUTS:
C           TJ    VALUE FOUND BY ROOT FIINDER
C           IER   ERROR CODE 0= ALL OK 1=  ITMAX COMPUTED, ABORT NEWTO
C                         2= DERIVATIVE BECAME ZERO, ABORT NEWTON
C
     IF( (IER.EQ.1) .OR. (IER.EQ.2) )THEN
     WRITE(9,334)IER,A,B,C,TJ,ITMAX
 334  FORMAT('**********************************************',//,
   $'   WARNING    IER= ',I3,' (2 MEANS DER 0   1 MEANS > ITMAX) ',/,
   $'A  B  C',3I9,'  TJ  ',F9.4 ,'  ITMAX',I9,/,
   $ '***************************************************',/)
     END IF
C
C     NOW USE TJ CACLUATED BY NEWTON TO PRINT OUT HEAT TRANSFER SUMMARY
C
     RD=THICK/(AREA(A,B)*COND)
C          UNITS: DEG K/W
C                 FROM ELLISON'S BOOK P. 6
C
     RV=1.0D0/(H(A,B)*AREA(A,B))
C          UNITS: DEG K/W
C                 FROM ELLISON'S BOOK P. 12
    DIFF = TJ-TW
    DIF4TH=TJ**4-TW**4
C
     RR=(TJ-TW)/(EPS(C)*AREA(A,B)*SIGMA*DIF4TH)
C          UNITS: DEG K/W
C                 FROM ELLISON'S BOOK P. 92
    QRR=(TJ-TW)/RR
```

```
      QRV=(TJ-TW)/RV
      QRD=(TJ-TO(A))/RD
      FRACD=QRD/POWER*100.0D0
      FRACV=QRV/POWER*100.0D0
      FRACR=QRR/POWER*100.0D0
      FRACT=FRACD+FRACV+FRACR

C     CALCULATE UNCERTAINTIES IN THERMAL RESISTANCES BASED ON KLINE & MCK
C
          WRD=( (WTHICK/ (AREA(A,B)*COND) )**2 +
     $        (-THICK*WAREA/(AREA(A,B)**2*COND))**2 +
     $        (-THICK*WCOND/(COND**2*AREA(A,B)))**2   )**0.50
          WRV=( (-WH/(AREA(A,B)*H(A,B)**2))**2 +
     $        (-WAREA/(H(A,B)*AREA(A,B)**2))**2   )**0.50
C
      DENOM = EPS(C)*AREA(A,B)*SIGMA*DIF4TH**2
      WRR=( (-WEPS*DIFF/(AREA(A,B)*EPS(C)**2*SIGMA*DIF4TH))**2 +
     $    (-WAREA*DIFF/(AREA(A,B)**2*EPS(C)*SIGMA*DIF4TH))**2 +
     $    (WTJTMP*(-3.0D0*TJ**4-    TW**4+4.0D0*TJ**3*TW) /
     $                                DENOM )**2+
     $    (WTW   *(-    TJ**4-3.0D0*TW**4+4.0D0*TJ**3*TW) /
     $                                DENOM )**2  )**0.50D0
C
C
      RRV=WRV/RV
      RRD=WRD/RD
      RRR=WRR/RR
C
      IF ((A.EQ.10).OR. (A.EQ.6)) THEN
      WRITE(9,225) R,WR,RRES,V,WV,RVOLT,TA,WTA,RTA,TO(A),WTO,RTO,TW,WTW,
     $ RTW,AREA(A,B),WAREA,RAREA,COND,WCOND,RCOND,
     $ THICK,WTHICK,RTHK,H(A,B),WH,RH,EPS(C),WEPS,REPS
C
  232 WRITE(9,235)A,B,C,WAREA,WH,EPS(C),
     $ RR,WRR,RRR,RD,WRD,RRD,RV,WRV,RRV,
     $ POWER,QRD,FRACD,
     $ QRV,FRACV,QRR,FRACR,FRACT
 235  FORMAT('  HEAT TRANSFER SUMMARY ',// ,
     $ 'LOOP COUNTERS  A= ',I3,5X,'  B= ',I3,5X,'  C= ',I3,/,
     $ 'VARIABLE   WAREA= ',F8.3, ' WH= ',F8.5, ' EPS(C)= ',F8.3,//,
     $ 'THERMAL RESIS. UNITS        VALUE      UNCERTAINTY    RATIO',/,
     $ '=======================================',
     $ '==========================',/,
     $ 'R RADIATION  DEG K / W   ',3(E10.5,3X),/,
     $ 'R CONDUCTION DEG K / W   ',3(E10.5,3X),/,
     $ 'R CONVECTION DEG K / W   ',3(E10.5,3X),///,
     $ 'POWER LOSS     UNITS        VALUE    PERCENTAGE OF TOTAL  ',/,
     $ '=======================================',
     $ '==========================',/,
     $ 'TOTAL INPUT    WATT      ',F8.3,/,'POWER OUTPUT:',/,
     $ ' CONDUCTION    WATT      ',F10.4,3X,F10.1,' %',/,
     $ ' CONVECTION    WATT      ',F10.4,3X,F10.1,' %',/,
     $ ' RADIATION     WATT      ',F10.4,3X,F10.1,' %',/,
     $ '                         ',15X,'--------',/,
     $ ' TOTAL OF FRACTIONS      ',13X,F10.1,' % ',////)
C
      IF( (A.EQ.6) .AND. (B.EQ.1) .AND. (C.EQ.1) )THEN
        HEAT=(TO(A)-TA)
        WRITE (3,236)TJ,HEAT.RR,RV,RD
 236  FORMAT ('* TJ= ',F9.4,/,
     $'*CIRCUIT TO MATCH UNCER4       SWM ',/,
     $'* TEST OUT CIRCUIT IN UNCER4 TO SEE IF UNCER4 MODELS  ',/,
     $'* CIRCUIT CORRECTLY                                  ',/,
```

```
      $'*  THE NOTES WRITTEN 10-7 SHOW DIAGRAM WITH NODE NUMBERS   ',/,
      $'*    PRINTED FROM UNCER4 FORTRAN                        ',/,
      $'VHEAT 1 0 ',F9.5,'                 ',/,
      $'IQ 0 2 0.90806                    ',/,
      $'*       THIS IS ELECTRICAL POWER PUT INTO CIRCUIT ',/,
      $  'RR 0 2 ',F15.8,/,
      $  'RV 0 2 ',F15.8,/,
      $  'RD 1 2 ',F15.8,/,
      $  '.END ')
C
       END IF
C
       END IF
C
C      BEGIN UNCERTAINTY CALCULATIONS FOR WTJ
C
       WI = ((WV/R)**2 + (-V*WR/R**2)**2)**0.5
       TTR = (1/RD + 1/RV + 1/RR)
       DV = I/TTR
       DI = V/TTR
       DTO = 1/(RD*TTR)
       DA = 1/(RV*TTR)
       DW = 1/(RR*TTR)
       TM = V*I + TO(A)/RD + TA/RV + TW/RR
       DR=(TM-TTR*TW)/((TTR*RR)**2)
       DVR=(TM-TTR*TA)/((TTR*RV)**2)
       DD=(TM-TTR*TO(A))/((TTR*RD)**2)
C                ABOVE FROM UNCER 2.1 NOTES P. 3
C
       WTOP=TO(A)-TO(1)
       WRITE(9,504)WTOP,TJ,A,B,C,QRD
 504   FORMAT('WTO= ',F9.4,'TJ= ',F9.4,' A B C =',3I5,'QRD = ',F9.4)
C
       WTJ(A,B,C) = ((DV*WV)**2+(DI*WI)**2+(DTO*WTOP)**2+(DA*WTA)**2+
      $(DW*WTW)**2+(DR*WRR)**2+(DVR*WRV)**2+(DD*WRD)**2)**0.5
C          ABOVE FROM UNCER 2.1  P. 1
C
C            MATCH COMPUTER'S NUMBER WITH HAND CALUCLATIONS TO CHECK
       IF ((A.EQ.10).OR. (A.EQ.6)) THEN
       WRITE(9,709)WI,TTR,DV,DI,DTO,DA,DW,TM,DR,DVR,DD,WTJ(A,B,C),A
 709   FORMAT(' WI= ',F9.5,' TTR= ',F9.3,' DV =',F9.6, /,
      $ ' DI= ' ,F9.3,' DTO= ' ,F9.3, ' DA = ', E9.3,'  DW =' ,E9.3,/,
      $ ' TM= ' ,F9.3,' DR = ' ,E9.3, ' DVR= ', E9.3,'  DD =' ,F9.3,/,
      $ ' WTJ= ' ,F9.3,'    A= ',I3,///)
       WRITE(9,505)WTOP,TJ
 505   FORMAT('WTOP= ',F9.4,'TJ= ',F9.4)
C
       T1=DV*WV
       T2=DI*WI
       T3=DTO*WTOP
       T4=DA*WTA
       T5=DW*WTW
       T6=DR*WRR
       T7=DVR*WRV
       T8=DD*WRD
       TJCHK= (T1**2 +T2**2+T3**2 +T4**2 + T5**2+T6**2+T7**2+T8**2)**0.5
C
       ST1=T1*T1
       ST2=T2*T2
       ST3=T3*T3
       ST4=T4*T4
       ST5=T5*T5
       ST6=T6*T6
```

```
      ST7=T7*T7
      ST8=T8*T8
C
      WRITE(9,909)T1,T2,T3,T4,T5,T6,T7,T8,TJCHK,TJ
 909  FORMAT( 'T1,T2,T3,T4,T5,T6,T7,T8,TJCHK    ',/,
     $  4(E10.5,5X),/,
     $  4(E10.5,5X),/,
     $  (F10.5,5X),'TJ= ',F10.5)
      WRITE(9,910)ST1,ST2,ST3,ST4,ST5,ST6,ST7,ST8
 910  FORMAT( 'ST1,ST2,ST3,ST4,ST5,ST6,ST7,ST8    ',/,
     $  4(E10.5,5X),/,
     $  4(E10.5,5X),/,
     $  (F10.5,5X),'TJ= ',F10.5)
      END IF
C
C     CALCULATE RATIOS OF UNCERTAINTY TO VALUE FOR PLOTTING
C        NOTE: VARIATION IN HEAT TRANSFER COEFFICIENT NOT CONSIDERED
C      WHP=H(A,B)-H(1,1)
      DIFP=(WTOP/WTJ(A,B,C))*100.0D0
C
  800 WRITE(10,810)A,B,C,WTOP,DIFP,WTJ(A,B,C)
  810 FORMAT(' ',3(2X,I3),3(3X,F13.6))
C
 1000 CONTINUE
C
 2000 CONTINUE
C
 5140 FORMAT('AXIS1',/,
     $' LENGTH= 3.7 IN  ',/,
     $'   LABEL=(F=SIMPLEX H=2 "WTO (DEG. K)") ',/,
     $'   ORDER  =  0. TO 4 BY 1.;'/,
     $' ',/,
     $'   AXIS2   ',/,
     $'   LENGTH= 4.4 IN ',/,
     $'   ORDER  =  50. TO 100. BY 10.   ',/,
     $'   LABEL=(A=90 F=SIMPLEX H=2 " WTO / WTJ (%) ");',/,
     $' PLOT DIFP*WTO /  HAXIS=AXIS1 VAXIS=AXIS2 FRAME ; ',/)
 5150 FORMAT('SYMBOL1 V=NONE  I=SPLINE L=1 C=RED;   ',/,
     2 'SYMBOL2 V=PLUS  I=SPLINE L=2 C=RED;   ',/,
     3 'SYMBOL3 V=X     I=SPLINE L=3 C=RED;   ',/,
     4 'SYMBOL4 V=Y     I=SPLINE L=4 C=RED;   ',/,
     5 'SYMBOL5 V=HASH  I=SPLINE L=5 C=RED;   ',/,
     6 'SYMBOL6 V=Z     I=SPLINE L=6 C=RED;   ')
      IF (C.EQ.1) THEN
      WRITE(10,5101)
 5101   FORMAT ('PROC GPLOT DATA= ONE UNIFORM; ')
      WRITE(10,5140)
      WRITE(10,5150)
      WRITE(10,5200)EPS(C)
 5200 FORMAT('TITLE1 " EMISSIVITY ',F7.4 ,' " ;'      )
      END IF
      IF (C.EQ.2)THEN
      WRITE(10,5108)
 5108   FORMAT ('PROC GPLOT DATA= TWO UNIFORM; ')
      WRITE(10,5140)
      WRITE(10,5150)
      WRITE(10,5200)EPS(C)
      END IF
      IF (C.EQ.3) THEN
      WRITE(10,5115)
 5115   FORMAT ('PROC GPLOT DATA= THREE UNIFORM; ')
      WRITE(10,5140)
      WRITE(10,5150)
```

```
      WRITE(10,5200)EPS(C)
      END IF
      IF (C.EQ.4)THEN
      WRITE(10,5122)
 5122   FORMAT ('PROC GPLOT DATA=  FOUR UNIFORM; ')
      WRITE(10,5140)
      WRITE(10,5150)
      WRITE(10,5200)EPS(C)
      END IF
      IF (C.EQ.5)THEN
      WRITE(10,5129)
 5129   FORMAT ('PROC GPLOT DATA=  FIVE UNIFORM; ')
      WRITE(10,5140)
      WRITE(10,5150)
      WRITE(10,5200)EPS(C)
      END IF
      IF (C.EQ.6) THEN
      WRITE(10,5136)
 5136   FORMAT ('PROC GPLOT DATA=  SIX UNIFORM; ')
      WRITE(10,5140)
      WRITE(10,5150)
      WRITE(10,5200)EPS(C)
      END IF
C
 6000 CONTINUE

      WRITE(10,6500)
 6500 FORMAT ('/*   ',/,'//   ')

 9999 STOP

      END

       SUBROUTINE NEWTON(DELTA,DDELTA,XINIT,ALPHA,ITMAX,ROOT,IER)
C        TAKEN FROM P 77  ATKINSON ELEM. NUMERICAL ANALYSIS
      INTEGER A,B,C
      PARAMETER (ZERO=0.0,ONE=1.0,TWO=2.0)
      IFLAG=1
      XO=XINIT
      ITNUM=1
 10   DENOM=DDELTA(XO)
      IF (DENOM.EQ.0.0)THEN
      IER=2
      ROOT=XO
      ITMAX=ITNUM-1
      RETURN
      END IF
      X1=XO-DELTA(XO)/DENOM
      DIF=X1-XO
      DUMMY=DELTA(XO)
      IF(ABS(X1-XO).LE.ALPHA)THEN
      IER=0
      ROOT=X1
      ITMAX=ITNUM
      RETURN
      END IF
      IF(ITNUM.LT.ITMAX)THEN
      ITNUM=ITNUM+1
      XO=X1
      GO TO 10
      ELSE
      IER=1
      ROOT=X1
```

```
      RETURN
      END IF
      END

      REAL FUNCTION DELTA(TJ)
      INTEGER A,B,C
      COMMON THICK,SIGMA,POWER,TA,TW,COND,A,B,C,
     $     AREA(20,10),EPS(6),H(20,10),TO(20)
      DELTA = POWER-(COND*AREA(A,B)/THICK*(TJ-TO(A)) + H(A,B)*AREA(A,B)*
     $         (TJ-TA)  +  EPS(C)*AREA(A,B)*SIGMA*(TJ**4-TW**4) )
      RETURN
      END

      REAL FUNCTION DDELTA(TJ)
      INTEGER A,B,C
      COMMON THICK,SIGMA,POWER,TA,TW,COND,A,B,C,
     $     AREA(20,10),EPS(6),H(20,10),TO(20)
      DDELTA = -(COND*AREA(A,B)/THICK + H(A,B)*AREA(A,B) +
     $            EPS(C)*AREA(A,B)*SIGMA*(4.0*TJ**3)  )
      RETURN
      END
```

The vita has been removed from the scanned document